LIMNOLOGY
and
OCEANOGRAPHY

ASLO

*Limnol. Oceanogr.* 00, 2017, 00–00

doi: 10.1002/lno.10549

# Flowpath and retention of snowmelt in an ice-covered arctic lake

**Alicia Cortés**,[1]* **Sally MacIntyre**,[1,2] **Steven Sadro**[1,a]

[1]Marine Science Institute, University of California, Santa Barbara, California
[2]Department of Ecology, Evolution, and Marine Biology, University of California, Santa Barbara, California

## *Abstract*

The extent to which snowmelt flowing into ice-covered lakes spreads horizontally and mixes vertically influences retention of solutes derived from the landscape. To quantify these transport processes and retention, we combine time series temperature and specific conductance measurements in Toolik Lake (Alaska) and its major inflow, with measurements of discharge and meteorology, and profiles of specific conductance, temperature, fluorescence, chlorophyll *a*, and dissolved organic carbon (DOC) in spring of 3 yr. During early snowmelt, the concentration of DOC in the stream was 750 $\mu$M, twice that in the lake. During slow melt (discharge ($Q$) $< 4$ m$^3$ s$^{-1}$), the incoming solute-rich intrusion spread lakewide below the ice. During melt with $Q > 6$ m$^3$ s$^{-1}$, the incoming water partially flushed the inlet basin and the more dilute water flowed over the original intrusion with a preferential flowpath to the outlet. Penetrative convection was restricted by the increased density gradients from the incoming plume and initially constrained to shallow mixing zones associated with the step changes in density. As ice thickness decreased to less than 1 m, heating caused density instabilities at the base of the intrusions that mixed solutes $\sim$ 10 m vertically, contributing to retention. Near-surface layers enriched with DOC persisted for $\sim$ 10 d during a rapid melt and for over 3 weeks when the melt was slow. Retention, of order 10–20%, also depended on the rapidity of melt and magnitude of discharge.

Springtime, with increased solar radiation and air temperatures, sets the stage for large changes in arctic lakes. Snow melting on the landscape enables discharge into the ice-covered lakes. Snowmelt is enriched in nutrients and dissolved organic carbon (Sickman et al. 2003; Cai et al. 2008; McNamara et al. 2008). Once sufficient lake ice melts near stream mouths, cold water can flow as an intrusion into the cold water immediately below the ice. Increased solar radiation warms and begins to melt the ice and, eventually, warms the water below. As near-surface waters warm, increased density, resulting because 4°C is the temperature of maximum density in freshwaters, induces penetrative convection that can erode the density structure formed over the winter (Farmer 1975; Salonen et al. 2014). Such mixing could entrain an incoming snowmelt plume to deeper depths. However, increased density differences due to melting ice or intrusions of fresher snowmelt and the water below can preclude penetrative convection (Pieters and Lawrence 2009). Increased solar radiation also warms the incoming stream water and modifies its density. Those changes, and the extent of vertical mixing near the stream mouth, will moderate the depth of penetration of the snowmelt inflow. Improvements in our understanding of plume dynamics and retention of introduced solutes require taking into account the various processes that moderate the density of both the lake and the stream.

Studies to date indicate that mixing between incoming snowmelt and lake water is limited. The region below the ice has been defined as a stratified boundary layer; temperatures are near 0°C immediately below the ice and increase to 1–2°C a meter away from the ice (Forrest et al. 2008; Kirillin et al. 2012). Bengtsson (1996) and Hamblin and Carmack (1990) found that incoming water occurred as a $\sim$ 1 m thick buoyant overflow with velocities $10^{-4}$ m s$^{-1}$ to $10^{-2}$ m s$^{-1}$ depending on discharge. Measured values of the coefficient of eddy diffusivity, $K_z$, were of order $10^{-5}$ m$^2$ s$^{-1}$ and would induce slow mixing (Bengtsson 1996). Tracers added below the ice prior to snowmelt were fully recovered downstream

*Correspondence: alicia.cortes@ucsb.edu

[a]Present address: Department of Environmental Science and Policy, University of California, Davis, California

Additional Supporting Information may be found in the online version of this article.

suggesting that snowmelt plumes would be through-flows (Bergmann and Welch 1985). Horizontal dispersion coefficients, $K_H$, associated with the plume in a 1 km$^2$ lake were low, $10^{-5}$ m$^2$ s$^{-1}$ to $10^{-4}$ m$^2$ s$^{-1}$, although plumes spread in the horizontal and sometimes completely across the lake (Stigebrandt 1978; Virtanen et al. 1979; Bengtsson 1996). Other processes could increase the spreading of an incoming plume. For example, dispersion coefficients of order $10^{-3}$ m$^2$ s$^{-1}$ to $10^{-2}$ m$^2$ s$^{-1}$ occurred when internal waves were present under the ice in lakes larger than 10 km$^2$ (Bengtsson 1986). Low flow speeds, strong density contrasts near the ice, and resulting low values of $K_z$ and $K_H$ suggest limited mixing of incoming plumes of snowmelt water with ambient water except where streams enter lakes. Unless other processes affect plume dynamics, incoming water could be seen as gradually filling a lake in the near surface boundary layer with slow subsequent drainage. In such a case, retention of the incoming waters would be minimal. The extent of retention will depend, however, on the extent to which mixing in the horizontal and in the vertical redistribute incoming solutes.

The goal of our study is to describe the stratification dynamics and the flowpath of incoming snowmelt and its retention in a moderate-sized, ice-covered, arctic lake in years that differ in weather and discharge. We describe the thermal, specific conductance and density structure prior to snowmelt and the subsequent changes with incoming snowmelt using moored instrument arrays and high resolution time series conductivity, temperature, depth (CTD) and fluorescence profiles on cross lake transects. Using specific conductance and fluorescence as tracers, we characterize the spatial and temporal evolution of plume waters, velocity of plumes, preferred flowpath, and retention within the lake. We illustrate how the weather influences plume dynamics through its influence on snow depth and related discharge, stream temperature, specific conductance, and density. We link the temporal changes in solute concentrations to attributes of the stream. We further illustrate the combined influence of changes in density of incoming plume waters, within lake heating, and ice thickness on the timing and depth of vertical mixing. Via these analyses, we provide new understanding of the mechanisms which enable retention of incoming water and solutes in an ice-covered arctic lake in spring.

## Study site

Toolik Lake, Alaska (68°38′ N, 149°38′ W), in the northern foothills of the Brooks Range, is an oligotrophic, multi-basin kettle lake with a surface area of 1.5 km$^2$, mean depth of 7 m, and maximum depth of 25 m (Fig. 1). It has four subbasins separated by shallow, 2–3 m deep ridges, one outlet in the north, and two primary inlets. Toolik Inlet, the larger of the two, enters from the south, and the smaller Toolik Inlet 2 (TI-2) enters from the northeast near the outlet. There are also several smaller streams that flow into the lake. The limnology of the lake is reviewed in O'Brien et al. (1997) and Luecke et al. (2014). MacIntyre et al. (2006, 2009) and Rueda and MacIntyre (2009, 2010) describe the surface energy budget, stratification, vertical mixing, horizontal circulation, fate of incoming stream water from high rainfall events, and links between physical limnology and primary productivity within the lake during the ice-free period. Whalen and Cornwell (1985) develop annual carbon and nutrient budgets for the lake including the contribution from snowmelt; Crump et al. (2003)'s study of microbial dynamics and community structure includes measurements of discharge and dissolved organic carbon (DOC).

## Methods and calculations

### Meteorology and discharge measurements

Meteorological data, obtained at a station 50 m to the east of the lake (Fig. 1), includes incoming and outgoing short- and long-wave radiation with a Kipp and Zonen CNR-4 radiometer; air temperature and relative humidity with a shielded and vented Vaisala HMP155A sensor; wind speed and direction with a RM Young 05103 and 05106 anemometer at 5 m height. Each sensor sampled every second, and data were averaged for 5 min. Changes in lake level were measured at a depth of 2-m with a pressure transducer (Druck, PDCR 930TI) every 10 min and stored as 3-h averages. Additional details on instruments specifications are found at http://toolik.alaska.edu/edc/abiotic_monitoring/instrumentation.php. Snowcover and depth were not measured in Toolik Lake's watershed; records are available from the nearby Imnaviat watershed (Euskirchen et al. 2012, http://aon.iab.uaf.edu/data_access). Bathymetric data to compute areas and volumes in the lake was collected with a Garmin GPSMAP 188 sounder and SonarMit echo sounder. Horizontal and vertical accuracy are 3 m and 0.5 m, respectively. The lake perimeter was determined with differential GPS. ESRI ArcGIS was used to process the bathymetric and GPS data, utilizing the 3D Analyst Tools to interpolate a continuous surface and generate volume and area measurements (J. Stuckey, unpubl. data).

Water level of Toolik Inlet was determined with a Stevens PGIII pulse generator and a float with data recorded on a Campbell Scientific CR510 data logger. Temperature and specific conductance were obtained with a Campbell 247 sensor with accuracy for temperature of 0.2°C and for conductivity 10% of the reading; results were stored in 30 min intervals. During spring 2015, we measured temperature with Onset Water Temp Pros (U22-001), specific conductance with Onset U24-001, and pressure with Onset U20L-001 loggers 500 m upstream of the Campbell system and sampling every 5 min. Temperature and specific conductance from the two sets of sensors were comparable and enabled us to extend the time series when gaps occurred.

We computed discharge of Toolik Inlet using two approaches. First, we utilized the within lake pressure measurements to compute $dV/dt$ from changes in lake surface

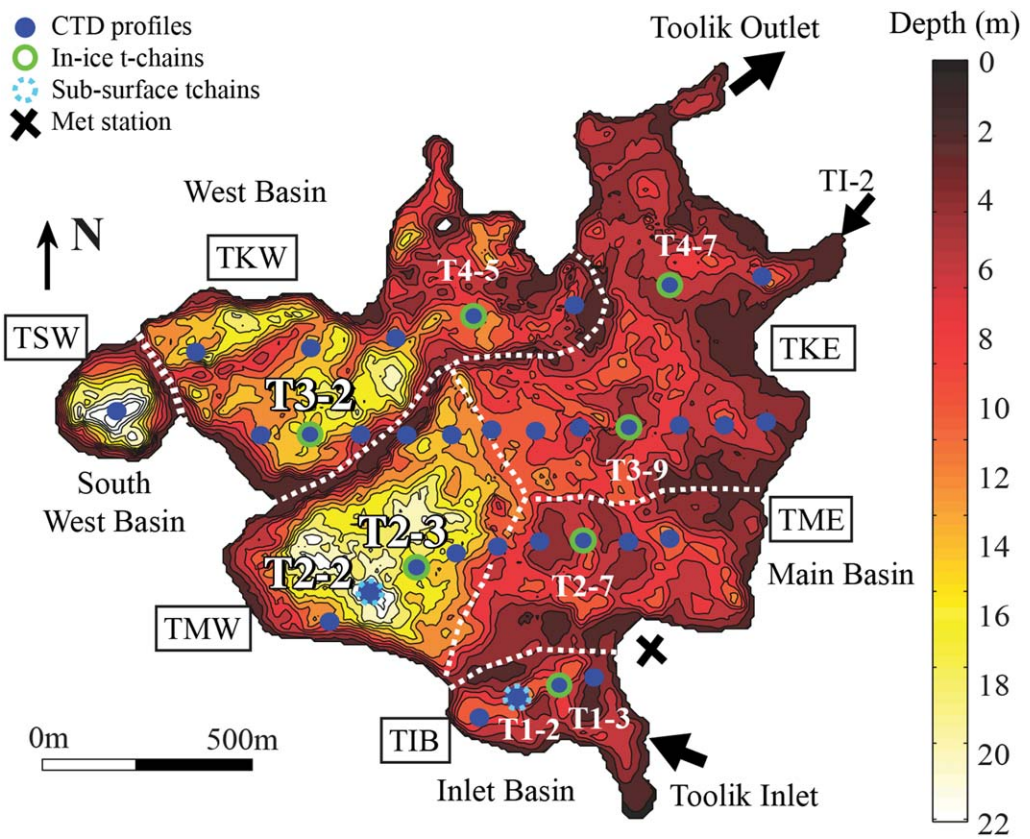


**Fig. 1.** Bathymetry of Toolik Lake, Alaska, with sub-basins defined based on the shallow moraines that separate them as Inlet Basin (TIB), the Main Basin which is further subdivided to describe the flow path as Toolik Main West (TMW), Toolik Main East (TME) and Toolik East (TKE), the West Basin (TKW), and the Southwest Basin (TSW). There are two inlet streams, the larger Toolik Inlet and a smaller one (TI-2) near the outlet. The blue dots mark the positions where profile data were taken on four cross-lake transects with numbering of transects from inlet to outlet, and holes on transects numbered from west to east. Sampling locations T1-2 and T2-2 are identified as TIB and TM, respectively, as these are sites of long-term deployments and are the locations of our sub-surface biogeochemical arrays. In-ice arrays were positioned at T1-3, T2-3, and T3-9 in all years. Contour intervals are 2 m.

elevation and discharge as $Q_{dz} = dV/dt + Q_{\text{out}}$, with $dV = A_s\, dz$, where $A_s$ is the surface area of Toolik Lake ($1.49 \times 10^6$ $m^2$), $dz$ is the change in surface elevation obtained from the pressure measurements, and the time interval $dt = 3$ h. The losses through the outlet $Q_{\text{out}}$ were assumed to have the same magnitude as incoming water from Toolik Inlet but delayed based on the time to flow across the lake, which we computed from our time series measurements of specific conductance under the ice (Table 1; Supporting Information Fig. 1S). Seepage near the outlet is unknown and causes an unaccounted for error. In the second approach, we computed discharge ($Q_h$) from changes in stage height ($h_1$, in m) in Toolik Inlet and a rating curve derived using flow rate estimates with a SonTek Flow Tracker in spring 2015. We applied the same rating curve for spring 2014. Obtaining accurate discharge measurements in early spring is difficult because stream waters flow into a small pond adjacent to Toolik Inlet for part of the period bypassing the pressure logger. Data are unavailable from the pressure logger until ice near the bottom of the stream melts. Hence, discharge cannot be computed from measurements of stage height during the initial period of snowmelt. Additionally, snowmelt flows over the ice on the lake, particularly along the margins, until ice near the mouth of the Inlet Basin has receded. The initial changes in lake surface elevation are based on the changes in pressure from the water flowing over the lake as well as the water flowing into the lake. Once the stream channel was ice free and flowed within the channel, we obtained similar estimates of discharge when computed from changes in surface elevation and stage. The similarity validates our estimates of magnitude despite the challenges in obtaining accurate estimates during springtime (Fig. 2p,q,r). In spring 2015 we measured temperature, specific conductance, and water level every 5 min at the second and smaller inlet, TI-2, using similar instrumentation from Onset, and estimated discharge using a salt dilution method (Moore 2005). We obtained discharge measurements at the outlet using the SonTek Flow Tracker.

### Moored instrumentation

Time-series measurements of temperature and specific conductance (SC) were measured on taut-line moorings with

**Table 1.** Estimates of discharge, flow velocity in the eastern and western basins, and advective time scale ($\tau_{adv} = l/u$ where $l$ is basin length and $u$ is flowspeed) under the ice based on changes in specific conductance (Supporting Information Fig. 1S). Discharge* is averaged over the time for the flow from the Inlet Basin (Site 1) to reach the sites to the east and west.

| | | Site 1 | Site 2 | dx (m) | Time 1 | Time 2 | Discharge, $Q$ ($m^3\ s^{-1}$) | Velocity to eastern basin $u_E$ ($m\ s^{-1}$) | Velocity to western basin $u_W$ ($m\ s^{-1}$) | $\tau_{adv}$ (d) |
|---|---|---|---|---|---|---|---|---|---|---|
| Spring 2013 | 1st Peak | T1-3 | T3-9 | 660 | 149 | 150.1 | 6.7 | 0.007 | | 2 |
| | | T1-3 | T2-3 | 448 | 149 | 150.4 | | | 0.004 | 3 |
| | 2nd Peak | T1-3 | T3-9 | 660 | 149.8 | 150.6 | 8.3 | 0.010 | | 1 |
| | | T1-3 | T2-3 | 448 | 149.8 | 150.4 | | | 0.009 | 1 |
| Spring 2014 | 1st Peak | T1-3 | T3-9 | 660 | 132.5 | 136.8 | 3.8 | 0.002 | | 7 |
| | | T1-3 | T2-3 | 448 | 132.5 | 137.9 | | | 0.001 | 12 |
| | 2nd Peak | T1-3 | T3-9 | 660 | 147.9 | 149 | 6.8 | 0.007 | | 2 |
| | | T1-3 | T2-3 | 448 | 147.9 | 149 | | | 0.005 | 2 |
| Spring 2015 | 1st Peak | T1-3 | T2-7 | 432 | 131.7 | 133.6 | 4.2 | 0.003 | | 4 |
| | | T1-3 | T3-9 | 660 | 131.7 | 134.6 | | 0.003 | | 4 |
| | | T1-3 | T4-7 | 920 | 131.7 | 135.3 | | 0.003 | | 4 |
| | | T1-3 | T2-3 | 448 | 131.7 | 135 | | | 0.002 | 7 |
| | | T1-3 | T3-2 | 765 | 131.7 | 137.4 | | | 0.002 | 7 |
| | | T1-3 | T4-5 | 908 | 131.7 | 135.5 | | | 0.003 | 4 |
| | 2nd Peak | T1-3 | T2-7 | 432 | 136.1 | 136.6 | 8.3 | 0.010 | | 1 |
| | | T1-3 | T3-9 | 660 | 136.1 | 136.9 | | 0.010 | | 1 |
| | | T1-3 | T4-7 | 920 | 136.1 | 137.2 | | 0.010 | | 1 |
| | | T1-3 | T2-3 | 448 | 136.1 | 136.7 | | | 0.009 | 1 |
| | | T1-3 | T3-2 | 765 | 136.1 | 137.3 | | | 0.007 | 2 |
| | | T1-3 | T4-5 | 908 | 136.1 | 137.4 | | | 0.008 | 1 |

* Velocity as a function of discharge at peak flows are: $u_E = [(1.7 \cdot Q + 4.5) \times 10^{-3}]$ ($R^2 = 0.99$) and $u_W = [(1.5 \cdot Q + 4.5) \times 10^{-3}]$ ($R^2 = 0.9$). Velocities at lower discharge do not follow these relations. Gray shading when not applicable.

a sub-surface float below the ice at T1-2 and T2-2 deployed before ice on each fall (Fig. 1). Temperature loggers were either RBR-1050, 1060, or Solos with 0.002°C accuracy and resolution an order of magnitude higher. Specific conductance loggers were a combination of RBR XR-420 and Onset U24-001 with resolution 1 $\mu$S $cm^{-1}$. Temperature (Onset Water Temp Pros with 0.1°C accuracy) and specific conductance (Onset U24-001) arrays were deployed in November of each year through the ice at T1-3, T2-3, and T3-9 (Fig. 1). The in-ice arrays extended from 0.5 m above the ice to 1.75 m below the surface of the ice. Instrument depths are indicated on the figures illustrating the data. In spring 2015, we deployed four additional Onset conductivity loggers 1.75 m below the ice surface at T2-7, T3-2, T4-5, and T4-7. Calibrations of RBR instrumentation are conducted at least every 2 yr. Conductivity and temperature loggers were intercalibrated against profiles with the JFE Advantech profiler described below in 2014 and 2015 and against a Hydrolab DS5 profiler in 2013. When additional accuracy was required, intercalibration was conducted using data from a temperature-gradient microstructure profiler deployed below the ice (PME Instruments, SCAMP). We merged temperature and specific conductance from neighboring in-ice arrays with under-ice arrays using data from the in-ice sensors when temperatures were above 0°C for a complete day which indicated the loggers were in the water as opposed to within the ice.

### Profiling

Profiles of conductivity, temperature, depth, turbidity, fluorescence, and dissolved oxygen were obtained along four transect lines (Fig. 1) with daily to weekly sampling. CTD profiles were obtained with a YSI CastAway in all years, with the data output from the instrument every 0.3 m. The CastAway averages data on the up and downcast which may cause gradients to smear if recovery is faster on the upcast. In 2014 and 2015, we used a JFE Advantech profiler with RINKO optical dissolved oxygen electrode deployed in free-fall mode with fall speed of $\sim$ 0.3 m $s^{-1}$. Vertical resolution was 0.1 m during spring 2014 and $\sim$ 0.025 m with continuous 10 Hz sampling in 2015. Data obtained in the holes in the ice were removed based on measurements of ice thickness when available or based on the depth of the first sharp gradient under the ice. Based on visual inspection of numerous profiles, we determined a temperature threshold of 0.7°C $m^{-1}$ and a threshold for specific conductance of

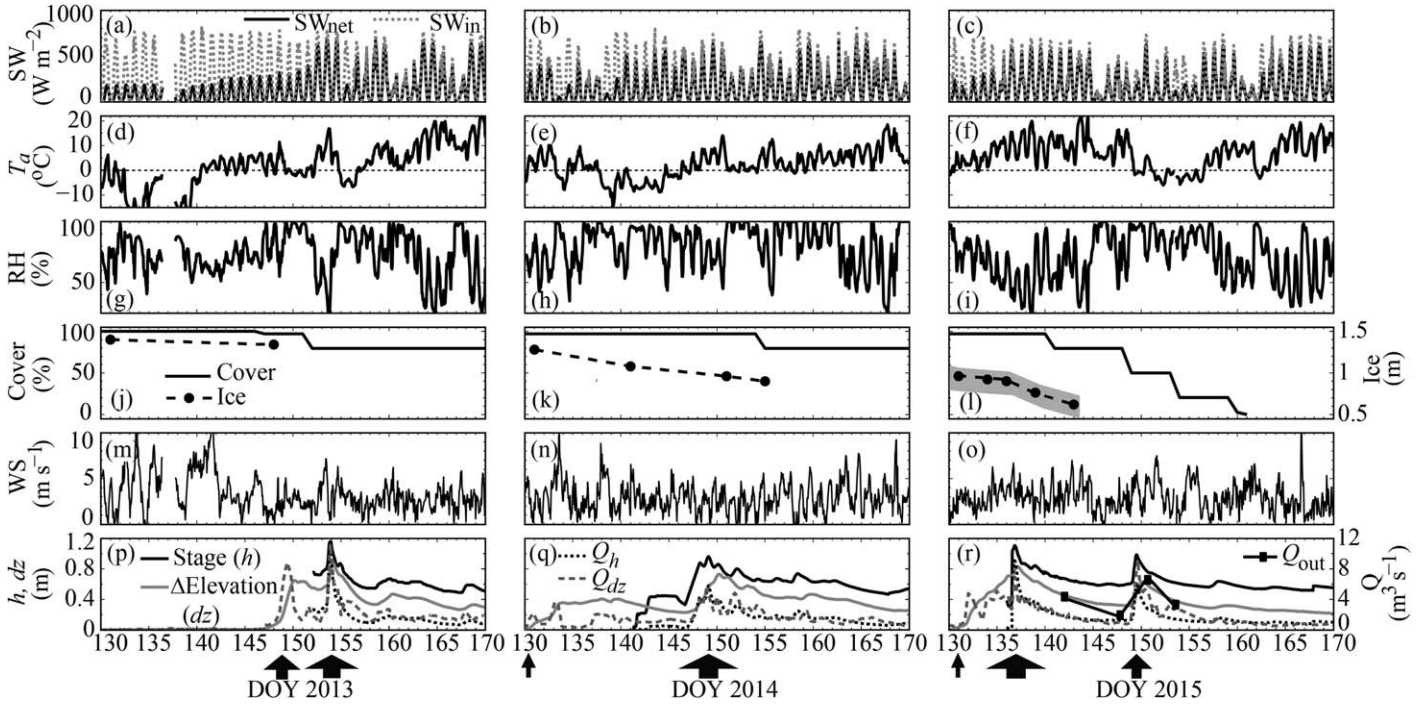


**Fig. 2.** Time-series of meteorological conditions during spring 2013, 2014, and 2015: (**a**–**c**) incoming and net short wave radiation ($SW_{in}$, $SW_{net}$), (**d**–**f**) air temperature ($T_a$), (**g**–**i**) relative humidity (RH), (**j**–**l**) percentage (%) of ice cover on the lake and ice thickness (-•-) at T2-3, with the shaded region indicating the full range of ice thickness across transect 2 in 2015, (**m**–**o**) wind speed (WS), (**p**–**r**) stream stage for Toolik Inlet (*h*), changes in surface elevation for Toolik Lake (*dz*), discharge computed from *h* and the rating curve from 2015 ($Q_h$), estimated discharge from *dz* ($Q_{dz}$), and outflow ($Q_{out}$). Arrows mark peaks in discharge from snowmelt with size relatively proportional to discharge in each year. Abrupt peaks in discharge from stage result once the anchor ice melts.

40 $\mu$S cm$^{-1}$ m$^{-1}$. CTD and irradiance profiles were obtained at least weekly with a Hydrolab DS5 water column profiler with LiCor 192SB collector.

### Chemical analysis

Discrete samples were obtained at T1-2 and T2-2 at least weekly prior to snowmelt and until the ice was unsafe for sampling. We obtained samples for DOC from Toolik Inlet in 2013 and 2015. We obtained additional samples for DOC at T1-3, T2-4, T2-7, T2-9, TI-2, and in the outlet stream in 2015. DOC samples were analyzed on a Shimadzu Total Organic Carbon analyzer following procedures in Carlson et al. (2010).

Samples for chlorophyll *a* (Chl *a*) were processed following Wetzel and Likens (2000). Samples were filtered through Whatman GFF filters within 24 h of collection and the filters frozen. Subsequently, the Chl *a* was extracted in 90% acetone in an ice bath at 0°C for 24 h prior to measurement on a calibrated Turner 10AU fluorometer. Values were corrected for phaeophytin by acidification. Major anions in lake water were measured using chemically suppressed ion chromatography on a Dionex ICS-900 ion chromatograph. Major cations were measured by inductively coupled plasma, optical emission spectroscopy on a Perkin-Elmer Optima 7300DV ICP-OES. Bicarbonate was computed from pH measured with the Hydrolab DS5 profiler and alkalinity measured by Gran titration. We obtained major ions in streams during snowmelt from the ARC LTER database.

### Calculations

Specific conductance, conductivity normalized to 25°C, was computed following Sengers and Watson (1986). We summed the major ions and bicarbonate to obtain salinity in mg L$^{-1}$, and obtained a factor *k* to compute salinity from specific conductance as, $S = SC \cdot k$, where *S* is measured salinity, SC is specific conductance in mS cm$^{-1}$, and *k* (mg cm L$^{-1}$ mS$^{-1}$) depends on the ion content in the water. For dilute snowmelt water, $k = 0.1$ with this coefficient applicable when SC < 0.020 mS cm$^{-1}$ and for lake water with slightly elevated major ions, $k = 0.9$. Density as a function of temperature and salinity was calculated following Chen and Millero (1977). The diffuse attenuation coefficient, $k_d$, was computed following Beer's Law using the irradiance data collected during weekly profiles.

We computed flow speeds of the incoming plume near peak discharge from the time series of specific conductance obtained by our in-ice arrays (Supporting Information Fig. 1S). We identified decreases in specific conductance from the movement of the plume and used the time interval and

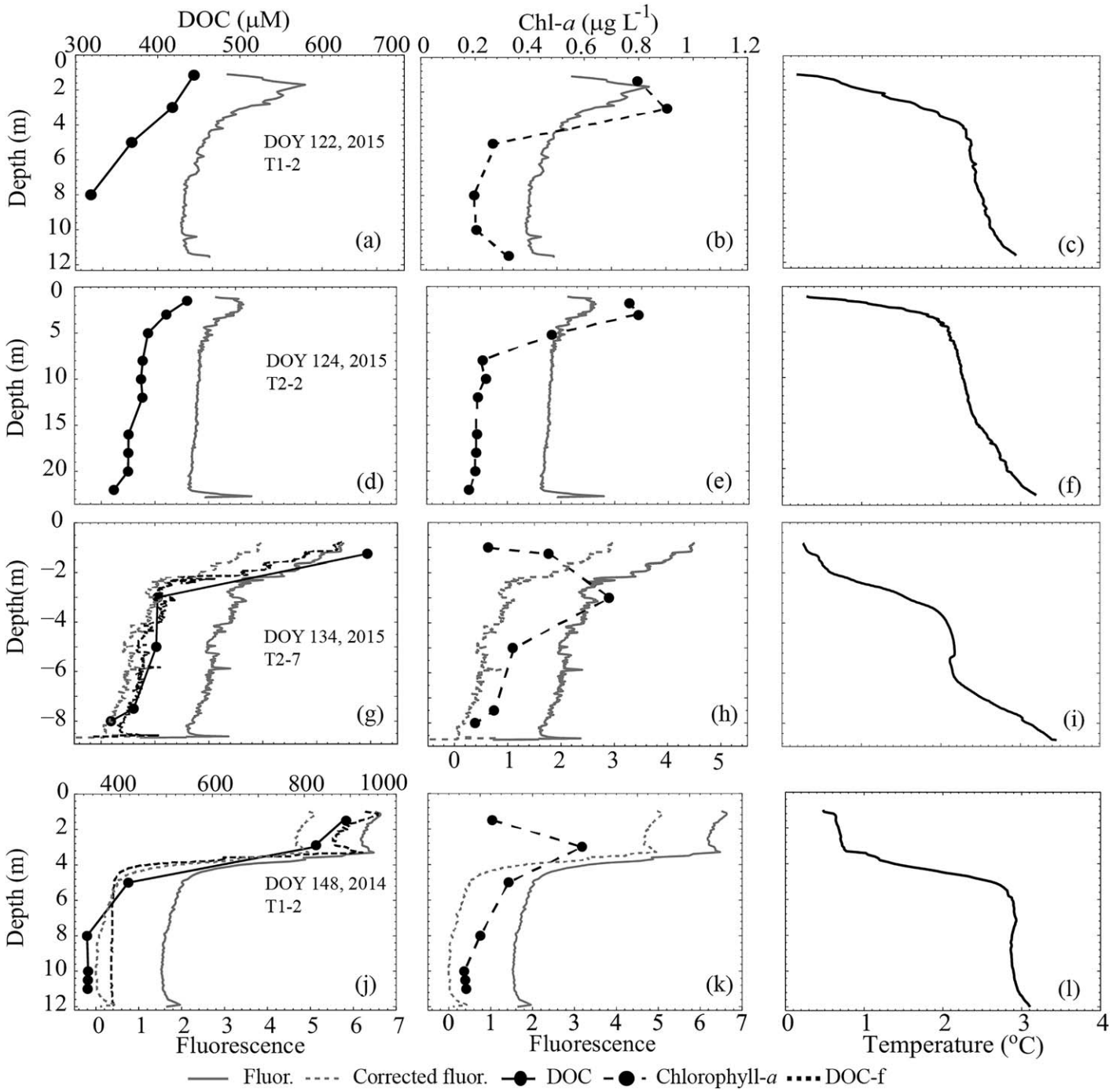


**Fig. 3.** (**a**–**f**) Profiles of fluorescence, dissolved organic carbon (DOC), Chl *a*, and temperature measured at sites T1-2 and T2-2 during the pre-snowmelt period (doys 122–124, 2015). (**g**–**l**) Profiles of fluorescence (fluor.), corrected fluorescence (corrected fluor.), measured DOC, DOC from corrected fluorescence (DOC-f), Chl *a*, and temperature during early snowmelt at sites T2-7 and T1-2 in 2015 and 2014, respectively. For locations, see Fig. 1.

distance between locations along the flowpath to estimate velocity (Table 1).

We assessed the contribution of DOC to the fluorescence signal from the JFE Profiler. Comparison of fluorescence readings on filtered and unfiltered water from the Inlet Basin in 2015 showed that less than 5% of the signal was due to Chl *a* after peak discharge. Prior to snowmelt, the magnitude of fluorescence was due to the combined effects of DOC and Chl *a* (Fig. 3a–f). We obtained the background fluorescence in the lake based on fluorescence values at depths where

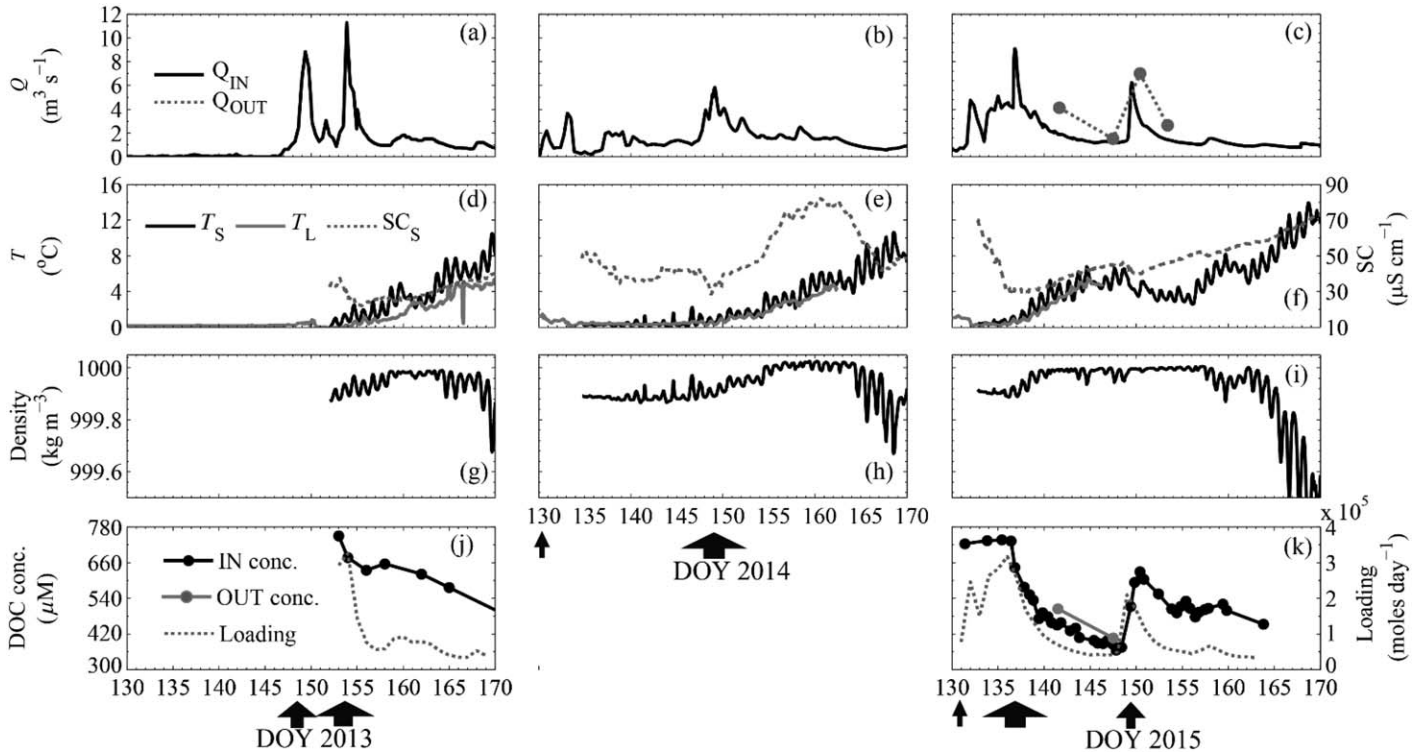


**Fig. 4.** Time series of (**a**–**c**) discharge ($Q_h$ when available and $Q_{dz}$ during the early period), (**d**–**f**) stream temperature ($T_s$), stream specific conductance ($SC_s$) and lake surface temperature at ~ 1.75 m below the surface of the ice ($T_L$), (**g**–**i**) stream density, (**j**–**k**) stream loading in moles per day and concentration of DOC for Toolik Inlet in 2013, 2014, and 2015. IN refers to data from Toolik Inlet with data from the outlet (OUT) when available. Arrows mark peaks in discharge from snowmelt.

DOC and Chl *a* concentrations were low; the background fluorescence ranged from 1.5 to 1.8. After snowmelt entered the lake, near surface values of Chl *a* decreased, and fluorescence was independent of Chl *a* (Fig. 3h,k). We subtracted a background value of fluorescence of 1.5 from the measured, and the remainder, corrected fluorescence, was contributed primarily by DOC (Fig. 3g–l). We regressed the corrected fluorescence signal (*fluo*) against measured DOC obtaining: DOC-f ($\mu$M) = $a \cdot \text{fluo}^2 + b$, where $a = 25.5$ and $b = 356.2$ (root mean square error, RMSE = 0.89) in 2014, and $a = 28.5$ and $b = 351.6$ (RMSE = 0.87) in 2015 (Fig. 3g,j). Maximal values of Chl *a* and DOC were within the near-surface boundary layer (Fig. 3c,f,i,l). We computed daily loading of DOC from Toolik Inlet by multiplying discharge times measured concentration which we interpolated to hourly intervals using a central difference scheme and summing the hourly values for each day.

## Results

### Meteorological forcing and discharge

Meteorological conditions and the extent of snow cover in May varied between years and led to differences in the timing and magnitude of discharge (Fig. 2). At the nearby Imnaviat basin, snow depth was 0.5 m in late April 2013 and 2014 and 0.7 m in 2015. May snowstorms increased snow depth to 0.7 m in May 2013. Mean air temperatures from 30 September to 30 April were −10.8°C, −8.2°C, and −7.4°C, in each year respectively. Ice thickness in early May of each year was 1.4 m, 1.3 m, and 1.0 m at T2-2 in the Main Basin and varied spatially by about 0.3 m (Fig. 2j–l). Ice-off occurred on doys 179, 174, and 161 (28 June 2013, 23 June 2014, and 10 June 2015).

Variability in weather led to between year differences in the timing and volume of discharge (Fig. 2). For example, temperatures near 0°C and the snowstorms in May 2013 led to persistent snow cover as indicated by low values of net short wave radiation vs. downwelling short wave radiation. As a result, inflows began 2 weeks later in 2013 than in 2014 and 2015. Discharge began to increase once air temperatures remained above 2°C for several days, and peaks in discharge were associated with air temperatures above 5°C (Fig. 2d–f). Two to three peaks in discharge occurred in May to early June of each year with peaks exceeding 8 $m^3\ s^{-1}$ in 2013 and 2015. Discharge decreased quickly after each peak. A late snowstorm led to a third peak in discharge in June 2015 (Fig. 2r).

Stream temperatures, specific conductance, and DOC varied with air temperatures and discharge (Figs. 2, 4). Stream temperatures were initially near zero and remained lower

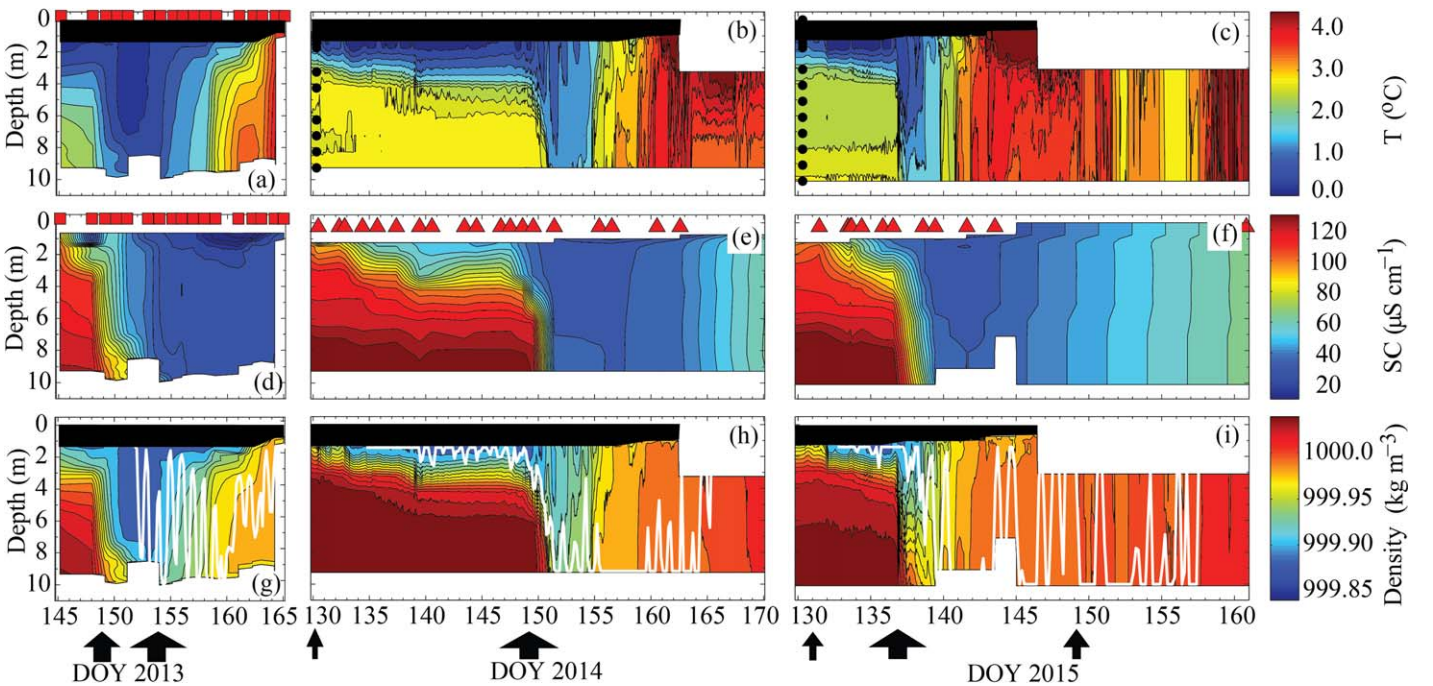


**Fig. 5.** Time series of temperature (**a**–**c**), specific conductance (**d**–**f**), and density (**g**–**i**) in the Inlet Basin (TIB) in 2013, 2014, and 2015. White lines on density plots show the expected depth of the intrusion based on the density of the stream. Red squares and triangles mark the dates when temperature and specific conductance from YSI CastAway profiles (red squares) and specific conductance from JFE Advantech CTD (red triangles) were interpolated to generate time series. Full ice cover and its change in thickness shown as black rectangles on top of the graphs of temperature and density. Black dots mark the depths of the temperature loggers; black arrows mark peak discharge and are scaled with the magnitude of discharge.

than 4°C through the peaks in discharge. Temperatures slowly rose thereafter, with variability caused by changes in weather. Specific conductance and DOC were higher at the onset of flow and decreased with increasing discharge. Specific conductance increased abruptly a few days after peak discharge in 2014. Maximal concentrations of DOC in Toolik Inlet were 750 $\mu$M in the early period and declined slowly in 2013 and more abruptly in 2015 to values slightly less than in lake water, $\sim$ 380 $\mu$M, after peak discharge. In contrast, maximal values in Whalen and Cornwell (1985) and Crump et al. (2003) were $\sim$ 1200 $\mu$M, dropped slightly at peak discharge and then increased to over 800 $\mu$M for at least 5 d. Specific conductance and DOC increased during the 3$^{rd}$ peak in discharge in 2015 (Fig. 4k). Density was initially 999.9 kg m$^{-3}$ and increased to 1000 kg m$^{-3}$ as the stream warmed to 4°C. However, due to increased specific conductance after peak discharge, density remained near 1000 kg m$^{-3}$ despite temperature fluctuations until temperatures increased above 8°C. Concentrations of DOC at the outlet were similar to those at the inlet, though obtained when discharge was low (Fig. 4k). Concentrations of DOC were similar to those in Toolik Inlet at TI-2, and discharge was an order of magnitude less at TI-2 (data not shown). Inputs of DOC from the landscape occurred during early snowmelt, increased on the rising limb of the subsequent peaks in discharge, and was sustained for some period of decreasing discharge (Fig. 4j,k).

**Stratification dynamics prior to and during snowmelt**

The stratification set up over the winter determines the depths at which snowmelt water will penetrate. Before snowmelt, temperatures in the Inlet Basin and Main Basin were inversely stratified with a sharp temperature gradient under the ice and a weaker gradient from 3 m to the bottom where, in the Main Basin, temperatures approached 3°C (Figs. 5, 6). A few days before discharge began, rising isotherms indicated heating had begun under the ice (Fig. 6a,c). The depth of the resulting penetrative convection varied. Specific conductance was higher just under the ice than in the water below due to cryoconcentration; it increased again in the lower water column. Density stratification between 3 m and 9 m was larger in 2014 than in the other 2 yr because of the larger gradients in temperature and specific conductance. Due to the contribution of solutes, as represented by specific conductance, to density, it was always greater than 1000 kg m$^{-3}$ below 3 m despite temperatures being less than 4°C. In fact, the dissolved ions doubled the density difference from the near surface to the lake bottom over that contributed by temperature. The density of lake water below the ice was larger than that of the stream water, and snowmelt initially was an overflow into both basins (Figs. 5, 6g,h,i, see pink line).

Incoming snowmelt initially freshened near-surface waters in the Inlet Basin enhancing near-surface density gradients

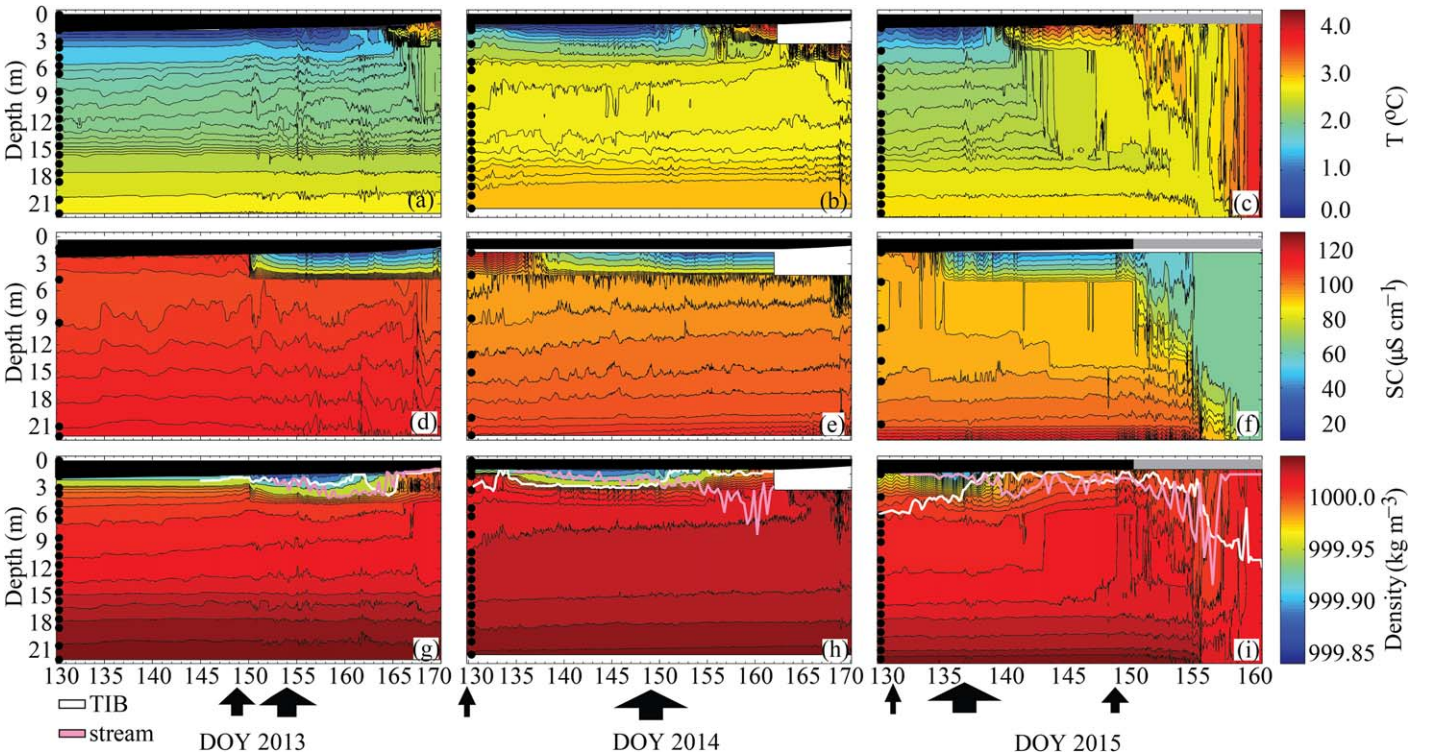


**Fig. 6.** As for Fig. 5, but at Toolik Main (TM) and with specific conductance based on data from moored arrays. Pink lines in panels (**g**, **h**, **i**) show the depth at which the stream would intrude based on its density, and white lines show the expected depth of the intrusion based on the mean density in the upper 3 m of TIB. The shift from stream water intruding to mixed water from TIB intruding occurs concurrently with the second peak in discharge in all 3 yr. Partial ice cover (gray rectangles). For more symbols, see Fig. 5.

(Fig. 5). Once discharge exceeded 6 $m^3$ $s^{-1}$, low temperatures and specific conductance $< 40$ $\mu S$ $cm^{-1}$ indicate that the Inlet Basin was flushed to an extent that it was primarily filled with stream water. After the second peak in discharge, the density of stream waters reached a maximum with diel variability superimposed as the stream warmed in the day and cooled at night (Fig. 4g–i). Consequently, the stream intruded below the surface in the Inlet Basin. Specific conductance increased at depth, and dilute, surficial water from the Inlet Basin, as opposed to the stream, flowed as a near-surface intrusion into the Main Basin (Figs. 4-6, white line). The increased salinity at depth stabilized the water column while temperatures were less than 4°C. Thus, at the end of sampling, a relatively warm, fresh layer overlaid cooler waters with slightly higher specific conductance in the Inlet Basin.

Fresher water flowing into the Main Basin either from the stream or as mixed water from the Inlet Basin increased the density gradient in the upper layers of the larger basin. This effect was evident shortly after the first peak in discharge as specific conductance in the near-surface layer under ice decreased and continued to decrease for some time afterwards (Fig. 6). The incoming water caused internal waves, evidenced by the increased amplitude and frequency of isotherm deflections at shallow and deeper depths, especially in 2013 (Fig. 6a). The persistent near-surface stratification indicated mixing from any resulting near-surface turbulence caused minimal vertical exchange with the water below. Based on its density relative to that of surface waters in the Inlet Basin, the intrusion resulting from the second peak in discharge would have flowed at shallower depths than the previous inflow (Fig. 6g,h,i). Thus, two distinct layers are expected from the incoming water from the two discharge events. Nearly 10 d after the second peak in discharge in 2013 and 2014 and within a few days of it in 2015, temperatures in the fresh upper layer warmed to $\sim$ 4°C. Rising isotherms indicative of mixing from penetrative convection occurred below the layer of warm, low density water in all 3 yr (Fig. 6a–c). The timing, duration and the depth of mixing varied due to differences in ice thickness and the density gradients below the near surface layer. The layer of warm, fresh water persisted near the surface in 2013 and 2014 until acted upon by additional mixing processes made possible by partial ice cover in the few days before ice off (data not shown). The final period in 2015 was slightly more complex as the warm layer was deflected downwards by the incoming and less dense waters from the third discharge event (Fig. 6c,f,i). In both the Inlet Basin and Main Basin, near surface layers with warmer, fresher water persisted until our final sampling at the end of the ice-covered period. In the Inlet Basin, the

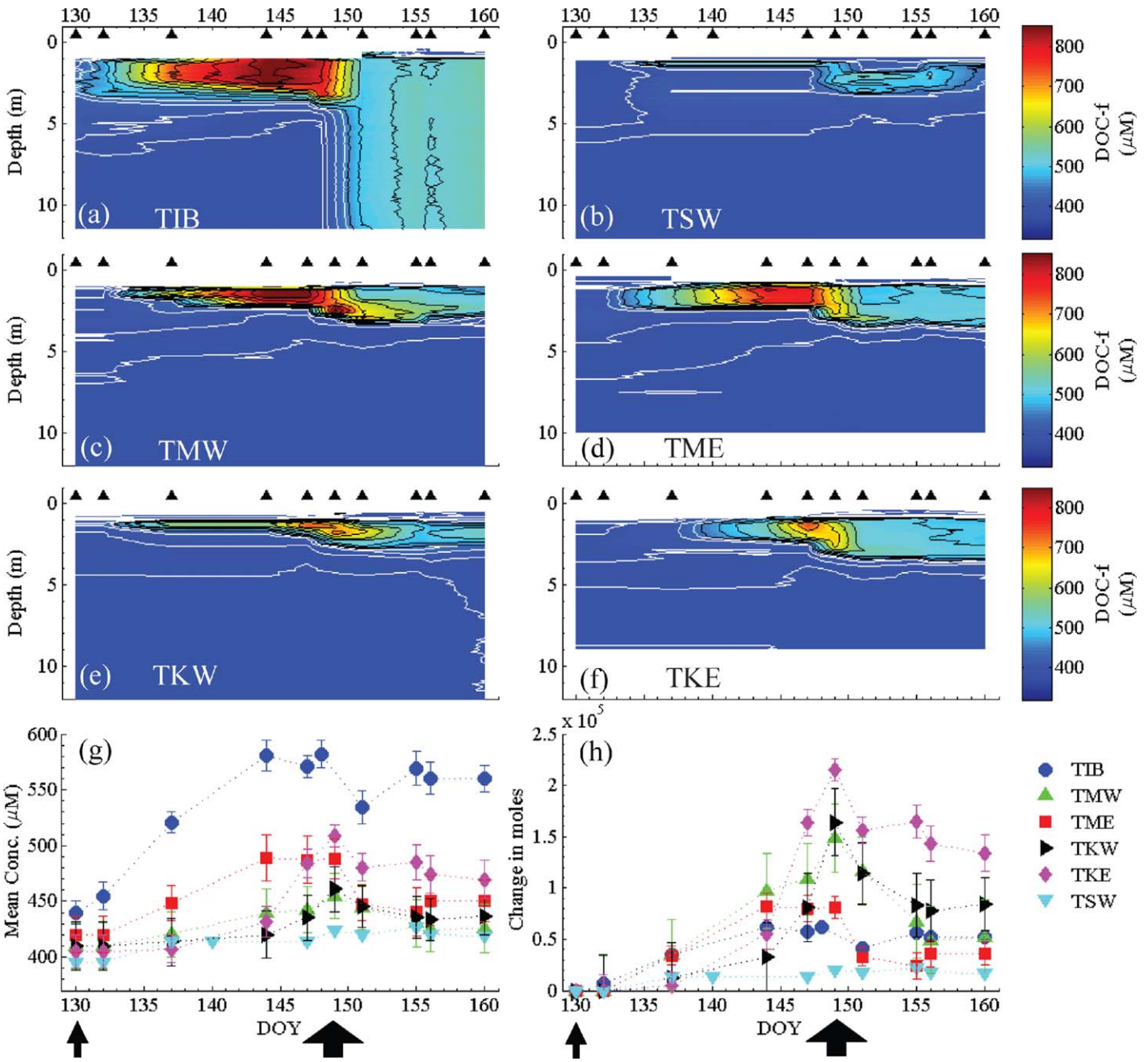


**Fig. 7.** (**a**–**f**) Time series of horizontally averaged profiles of DOC-f in 2014: (**a**) Inlet Basin, TIB, (**b**) South West Basin, TWS, (**c**) Main West, TMW, (**d**) Main East, TME, (**e**) Toolik West, TKW, and (**f**) Toolik East, TKE. (**g**) Time series of mean concentration of DOC-f and (**h**) time series of change in moles of DOC-f (total minus initial value) in the six basins. Arrows mark the peaks in discharge. Symbols overlap on the first few sampling days but magnitudes can be determined by the dashed lines.

stability was provided by a plunging inflow with higher specific conductance. In the Main Basin, it was provided by overflows of fresher water.

### Spatial variability of intrusion depth and solute concentrations

The vertical dimension of the plume and the concentrations of DOC-f within it varied among basins with patterns similar to those obtained from our time series data in the Main Basin (Figs. 7, 8). In 2014, with the slower melt, horizontally integrated concentrations of DOC-f in Toolik Lake's sub-basins as defined in Fig. 1 increased over the first 2 weeks to 800 $\mu$M in a layer below the ice (Fig. 7a–f). The intrusion's vertical dimension was up to 4 m in the Inlet Basin and thinned across the lake. Concentrations within the intrusion were similar to those in the Inlet Basin in the

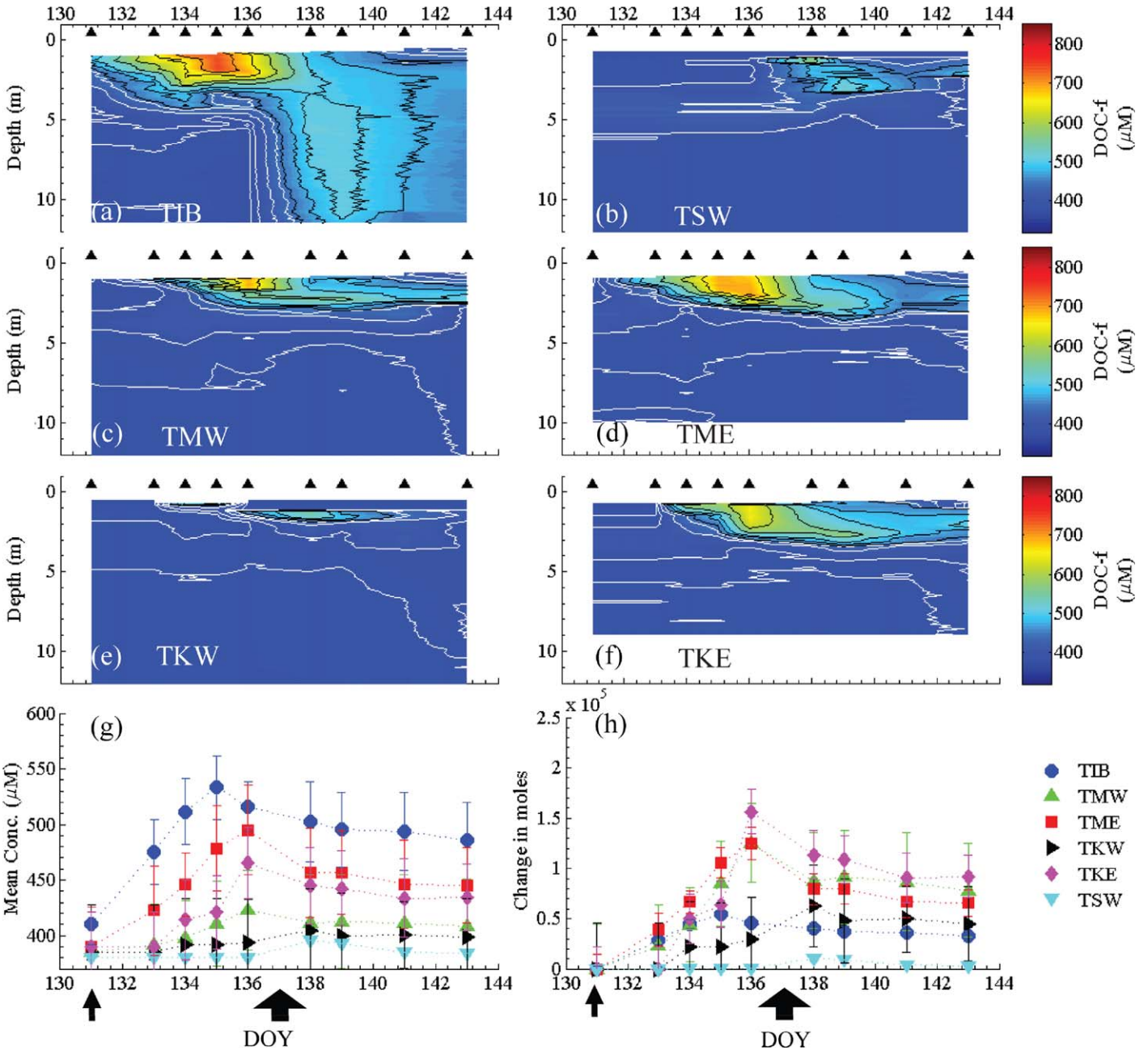


**Fig. 8.** As for Fig. 7 except for 2015.

western half of the Main Basin but lower elsewhere. During the second peak in discharge, the incoming DOC-f mixed with water in the Inlet Basin and this mixed water with concentrations greater than 500 $\mu$M then flowed offshore. As expected from the changes in density of the incoming stream relative to that in the Inlet Basin, water from the Inlet Basin flowed above the original plume water across the lake (Figs. 6h, 7). Thus, two layers with distinct concentrations of DOC-f were created. Within a few more days, the layering was still present in the western basins but was reduced in the eastern ones where the vertical dimension of the overall intrusion had increased. This difference implied greater flow to the east, as supported by velocity calculations (Table 1), and more vertical mixing. The progressive decline in near surface concentrations in TKE results from the transport of the initially mixed water in the Inlet Basin to TME and then to TKE. The pattern in 2015 was similar to that in 2014 except that concentrations of DOC-f were lower, the mixing of DOC-f within the Inlet Basin was not complete, and layering persisted in the eastern basins for at least 8 d after peak discharge (Fig. 8a–f).

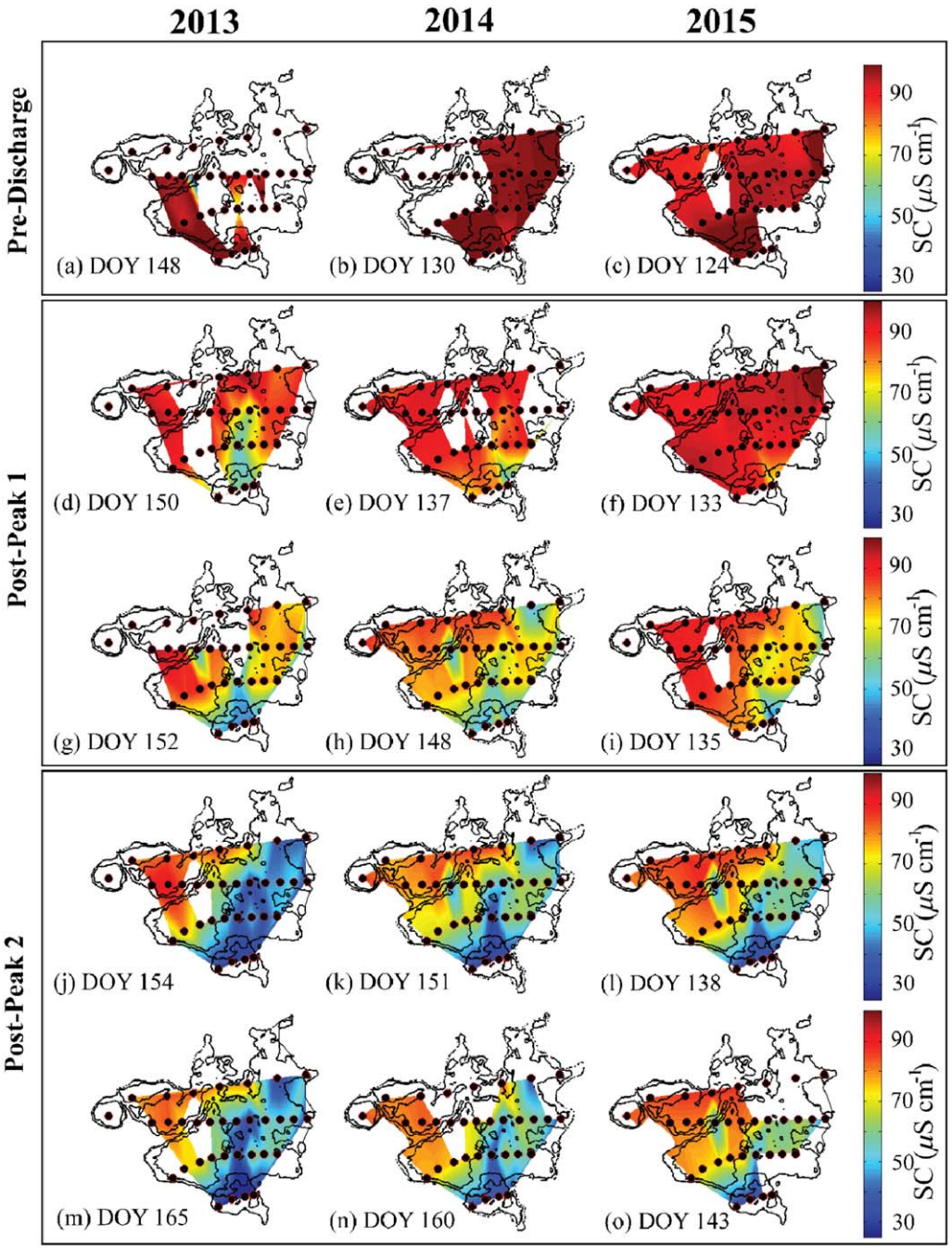


**Fig. 9.** Horizontal distribution of specific conductance (SC) integrated over the upper 5 m during spring 2013, 2014, and 2015 (vertical panels) (sampling date as doy is within each subplot): (**a**–**c**) prior to snowmelt; (**d**–**f**) right after the first and smaller peak in discharge; (**g**–**i**) before the second, and larger, peak in discharge; (**j**–**l**) after the second peak in discharge; and (**m**–**o**) final date of sampling. See Fig. 2 for peak discharge dates.

Between year variability in the concentrations of DOC-f that flowed from the Inlet Basin resulted from differences in the extent of vertical mixing during and after the second peak in discharge and changes in the concentrations in the incoming stream (Figs. 4, 5). DOC-f was well mixed in the Inlet Basin in 2014 but only partially mixed in 2015 after the second peak in discharge (Figs. 7a, 8a). Additionally in 2014, DOC-f decreased just after peak discharge and increased again 5 d later. We infer that the increase was caused by increases in DOC in the stream coincident with its warming and increased specific conductance. This inference is supported by Whalen and Cornwall's (1985) and Crump et al.'s (2003) earlier observations of increased DOC after peaks in discharge. In 2015, concentrations in the Inlet Basin

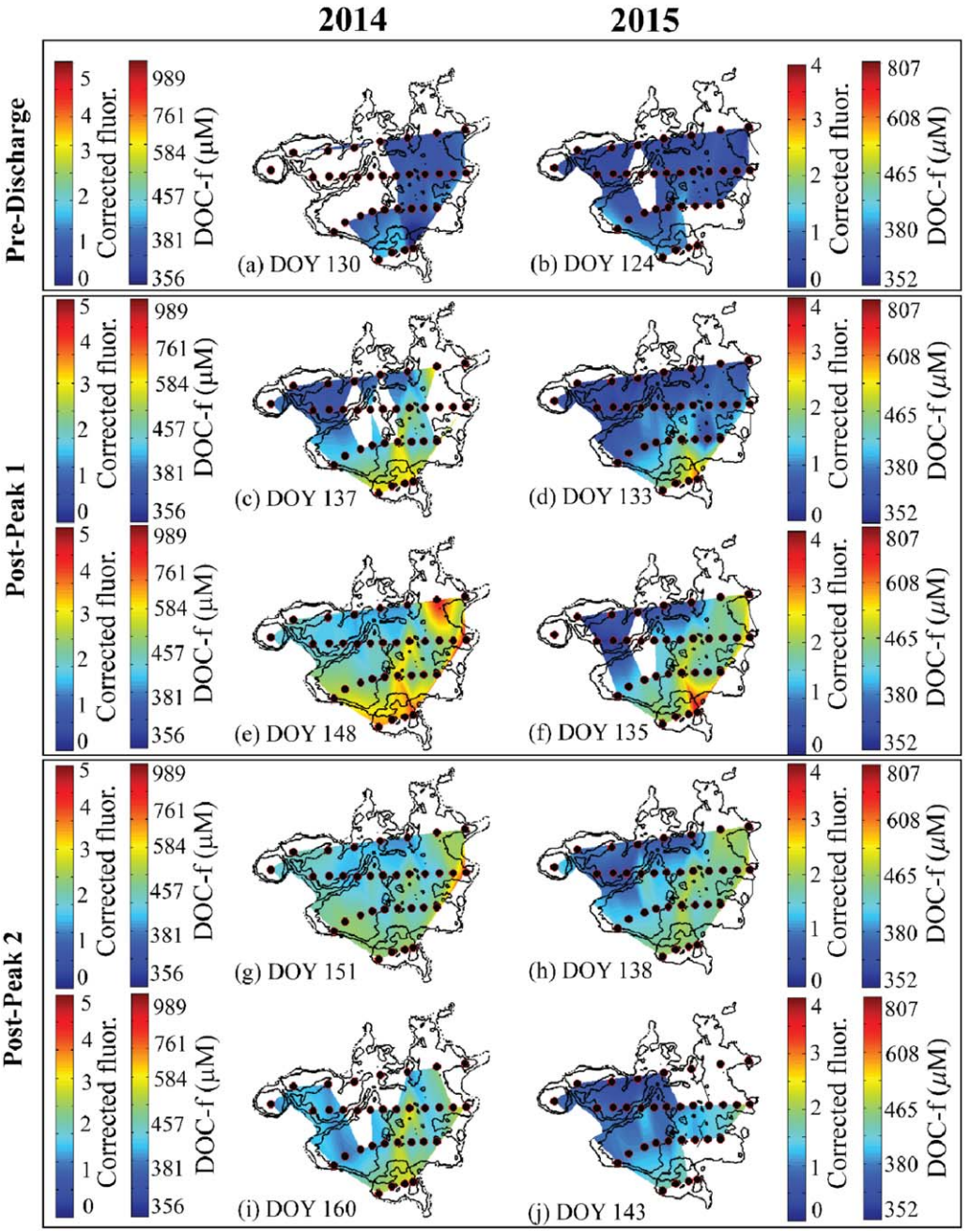


**Fig. 10.** As for Fig. 9, except corrected fluorescence (corrected fluor.) and DOC-f integrated over the upper 5 m in spring 2014 and 2015. Note change in scale bars each year.

and the stream decreased after peak discharge with the lowest values near the surface. The between year differences in vertical mixing moderated retention in the Inlet Basin.

### Spatial-temporal variability of plume water in the horizontal

Incoming snowmelt added DOC-f and freshened the near-surface water. Spatial patterns in the near surface, as obtained by integration over the upper 5 m, were initially created in the Main Basin due to greater flow where the moraine, which separates the Inlet and Main Basins, was deeper (Figs. 1, 9, 10). Marked differences in specific conductance occurred among years (Fig. 9). In 2013, with a high first peak in discharge, a preferential flow path developed immediately with freshening on a path to the outlet (Fig. 9d; Table 1). In contrast, freshening over the full lake was greatest in 2014 with the initial 3 week period of modest discharge (Fig. 9h). Dilution to the east intensified after the

**Table 2.** Transport processes under the ice, associated velocities ($u$) or eddy diffusivities ($K_z$), length scales ($l$), and time scales and their definitions. When $\tau_{rho}$ and $\tau_{mix}$ are $<= \tau_{adv}$, horizontal flows and vertical mixing can act to moderate the distribution of solutes and particulates while the plume traverses the lake.

| Process | Velocity (m $s^{-1}$) or $K_z$ ($m^2$ $s^{-1}$) | Length scale (m) | Time scale | Time (d) |
|---|---|---|---|---|
| Advection from the plume | 0.01 | 1000 | $\tau_{adv} = l/u$ | 1 |
| under the ice | 0.002 | 1000 | | 6 |
| | 0.001 | 1000 | | 12 |
| Advection from horizontal | 0.004 | 100–300 | $\tau_{rho} = l/u$ | 1 d or less |
| density differences | 0.012 | 100–300 | | Few hours |
| Vertical mixing ($K_z$)* | Within intrusion $5 \times 10^{-6}$ | 0.5 | $\tau_{mix} = l^2/K_z$ | ~0.5 |
| | Base of intrusion $1 \times 10^{-4}$† | 3 | | 1 d |

* Units of $K_z$ are $m^2$ $s^{-1}$.
† Only occurs once irradiance is sufficient at the base of the intrusions.

second peak in discharge in all years (Fig. 9j,k,l). Cross basin contrasts were larger in years with a shorter interval between peaks in discharge; subsequent horizontal spreading was evident by decreases in specific conductance in the far west or southward movement of water with higher specific conductance by the end of sampling (Fig. 9m,o).

Near surface DOC-f initially increased as specific conductivity decreased, which was indicative of loading from the landscape (Figs. 2, 9, 10). Horizontal spreading was greater in 2014 with its longer period of slow discharge. After the 2nd peak in discharge, DOC-f decreased due to inputs of water from the Inlet Basin where stream water had mixed with lake water (Figs. 5, 7, 8). As was observed with specific conductance, the preferential flowpath was more pronounced in 2015 than 2014.

### Flow speeds

Flow speeds of the incoming plume depended on discharge, $Q$ (Supporting Information Fig. 1S; Table 1). When $Q$ was ~ 4 $m^3$ $s^{-1}$, as for the first discharge event in 2014 and 2015, flow speeds to the east and west were a few millimeters per second. When peak discharge first reached values in excess of 6 $m^3$ $s^{-1}$ and snowmelt water mixed with that in the Inlet Basin (Fig. 5), velocities were higher and elevated by a few mm $s^{-1}$ to the east, suggesting a preferred flowpath toward the outlet. When $Q > 8$ $m^3$ $s^{-1}$ and $Q$ in a previous peak exceeded 6 $m^3$ $s^{-1}$, as in 2013, velocities reached 0.01 m $s^{-1}$ and were the same to the east and west. The computed velocities at lower discharge are similar to those reported in earlier studies (Bengtsson 1986; Hamblin and Carmack 1990). The more extensive array deployed in 2015 extended our understanding of plume dynamics. At peak flow, speeds remained constant along each trajectory and flow was slightly faster to the east at higher discharge (Table 1). After decreases associated with passage of the plume, specific conductance returned to the high values present prior to snowmelt in TKW (data not shown). Thus, the more extensive array provided evidence for a meandering plume in the far western basin.

Velocity increased linearly in the east basin as discharge increased. To the west, the rate of increase was lower until speeds increased at the highest discharges measured. Since $Q$ decreased to values below 2 $m^3$ $s^{-1}$ after the peaks, flow speeds would have decreased to even lower values than we measured. Hence, over the course of the spring, flows were unsteady with faster flows during peaks in discharge and with slower and, at least sometimes, meandering flows later. The time scale for the plume to cross the lake, that is $\tau_{adv}$, varied from 1 d to 7 d to the east and 1–12 d to the west (Tables 1, 2). When $\tau_{adv}$ is rapid, considerable losses would occur from the lake. However, when $\tau_{adv}$ is long, processes with more rapid time scales could moderate the distribution of solutes.

Velocities due to density differences in the horizontal are computed as: $u_x = (g' h)^{1/2}$, where $g'$ is the reduced density ($=g \Delta\rho/\rho$), $g$ is the gravitational acceleration, $\Delta\rho$ is the horizontal density gradient, and $h$ is the thickness of the density driven flow (Sturman et al. 1996). Conditions conducive to density driven flows were set up by the preferential flow path, the spatial differences in specific conductance due to the meandering plume, and, as previously quantified by Mironov and Terzhevik (2000), spatial differences in ice thickness which lead to differences in temperature under the ice. For example, ice thickness by doy 143 in 2015 was 70 cm at some stations and 35 cm at others, with reduced ice cover where bathymetry shoaled. Density differences, $\Delta\rho$, between pairs of profiles in the western basins were of order 0.002 kg $m^{-3}$ and 0.012 kg $m^{-3}$. Assuming $h \sim 1$ m, $u_x \sim 0.004$ m $s^{-1}$ and 0.012 m $s^{-1}$. These horizontal flows are similar to flow speeds of the incoming plume. On the scale of the distances between measurements, 100 m, and on distances between basins, ~ 300 m, the time scale for advection from horizontal density differences, $\tau_{rho}$, ranged from a few hours to a day, less than or equal to $\tau_{adv}$ (Table 2). Interleaving of water masses was possible then at high and at low discharge, and as was particularly noticeable after the second peak in discharge, would reduce vertical gradients within intrusions while simultaneously redistributing introduced solutes horizontally.

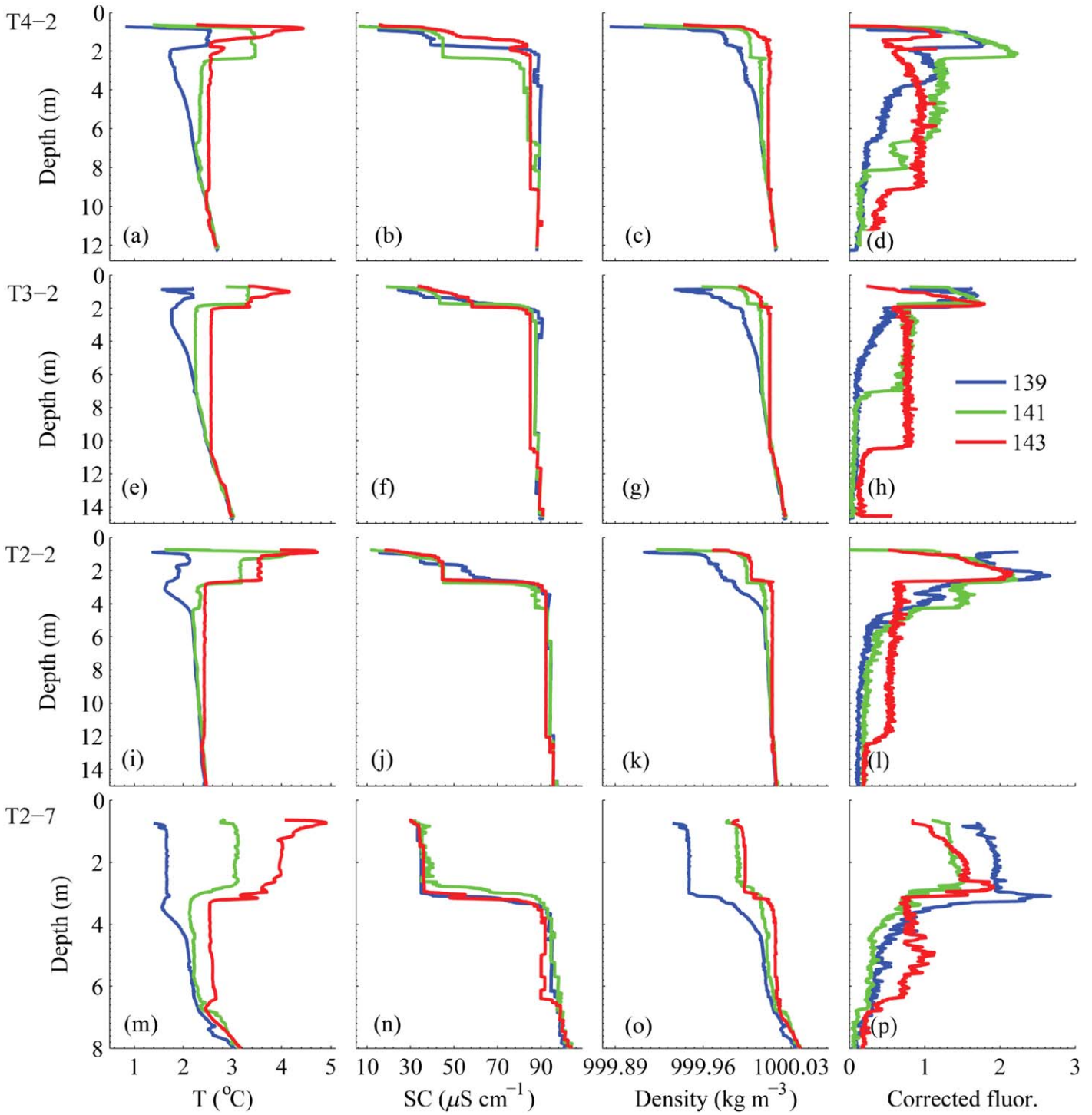


**Fig. 11.** Profiles of temperature (T) specific conductance (SC), density, and corrected fluorescence (Corrected fluor.), on doys 139, 141, and 143 in 2015 at (**a**–**d**) T4-2; (**e**–**h**) T3-2; (**i**–**l**) T2-2 (TM), maximum depth 22 m; and (**m**–**p**) T2-7. For locations, see Fig. 1.

**Vertical mixing**

The penetrative convection which occurred prior to snowmelt was arrested in the surface boundary layer and below by the incoming plume with its greater density contrasts (Fig. 6). Within the surface boundary layer, heating and internal wave motions induced some mixing (Fig. 11). Penetrative convection occurred below the lens of fresher water beginning after the second peak in discharge (Figs. 6, 11).

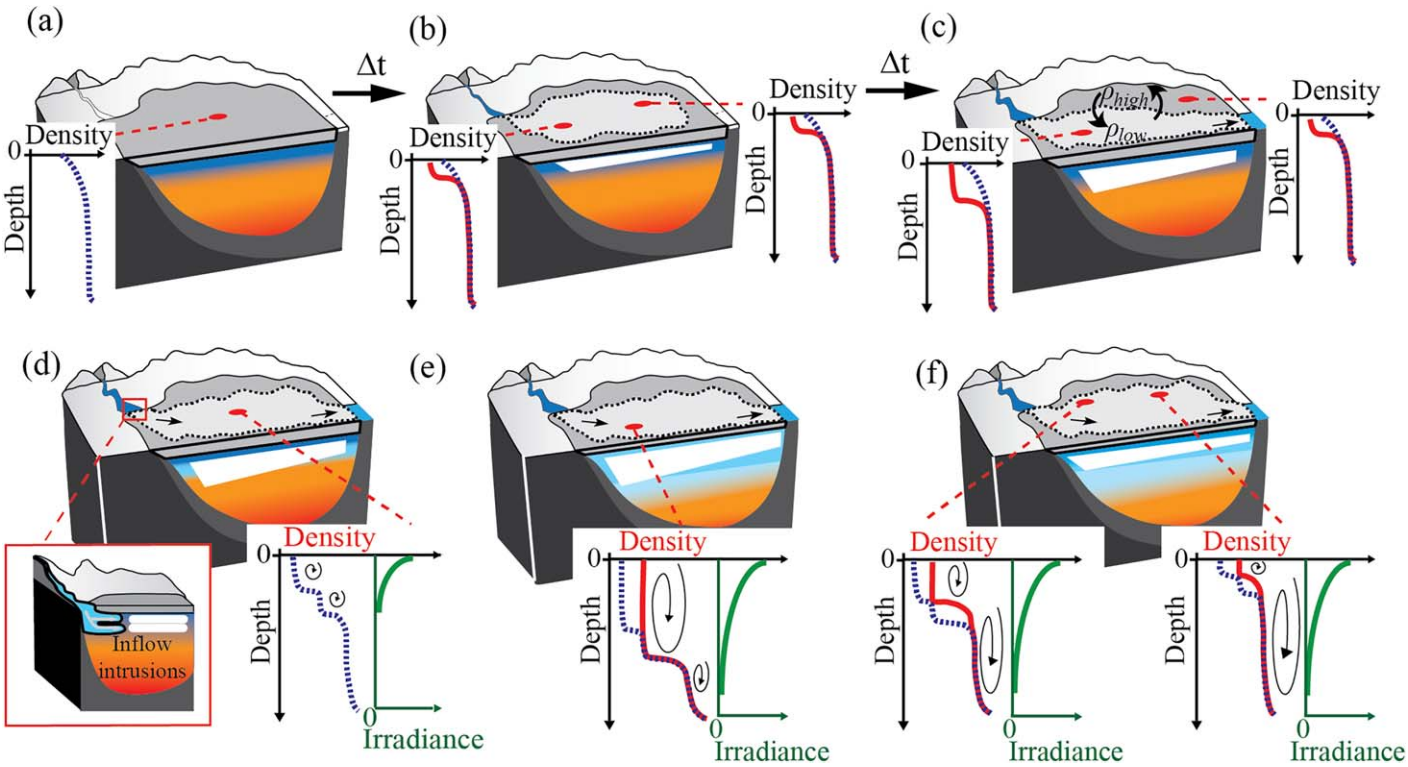


**Fig. 12.** Upper panels: Schematic illustrating the changing flowpath of snowmelt under the ice with (**a**) initial density structure under the ice and changes in density structure after (**b**) a relatively low first and a (**c**) higher second peak in discharge. Lower panels: Depth of penetrative convection as a function of irradiance and spatial variability in plume thickness for (**d**) initial and subsequent flow (**e**) on preferential flow path where the initial upper layer thickness is deeper due to the plume's momentum, and (**f**) with distance from the mouth of the stream and away from the preferential flowpath. Lighter gray within the plume is indicative of fresher, less dense water ($\rho_{low}$) as opposed to higher density water ($\rho_{high}$). Blue dashed line is initial density profile and red is a subsequent one at each location. Penetrative convection, as indicated by uniform density and curves representing eddies, extends deeper where plume thickness is shallower (**f**, right profile).

Heat and solutes were mixed downwards. The depth of mixing was greater in 2013 and 2015 than in 2014. The deeper penetrative convection began earlier in the far west where the intrusion was thinner and in the eastern basins where the plume's inertia was stronger (Fig. 11). Once started, it caused progressively deeper mixing. These patterns are illustrated schematically in Fig. 12d–f. Occasionally overflows of water with higher specific conductance were observed in the far western basin which may also have contributed to penetrative convection (Fig. 11b,f). Such overflows may have been induced by horizontal density differences from the meandering plume.

We verified that heating of water below 3 m could cause the deeper mixing observed in 2015 by computing irradiance under the ice from the incoming shortwave radiation, the resulting heating at different depths and changes in density, and the formation of instabilities. From our measured profiles of irradiance, the diffuse attenuation coefficient of ice, $k_{d\_ice}$, was 2 $m^{-1}$, and in the water $k_d$ was 0.6 $m^{-1}$. We modeled the onset of a sufficient increase in density to drive penetrative convection below 3 m as observed on day 141 at T3-2 by letting the albedo at the surface of the ice be 0.5 and using our measured values of attenuation. We additionally modeled it using an albedo of 0.2 as occurs toward the end of the ice-covered period (Kirillin et al. 2012). For the lower reflection, instabilities would be induced for $k_{d\_ice} = 3\ m^{-1}$, and $k_d = 0.7\ m^{-1}$. These higher values are reasonable given that our profile data was obtained below holes in the ice and based on other observations of $k_{d\_ice}$ in spring (Jakkila et al. 2009). The increased irradiance that initiated the instabilities at 3 m was 2–3 W $m^{-2}$.

Time scales of vertical mixing $\tau_{mix}$ are computed as $l^2/K_z$ where $l$ is the depth over which mixing occurs and $K_z$ is the coefficient of eddy diffusivity. We computed the density flux under the ice and from that $K_z$ following Jassby and Powell (1975). This approach has been used at Toolik Lake and other lakes under ice free conditions (MacIntyre et al. 1999, 2009). $K_z$ was maximally of order $5 \times 10^{-6}$ $m^2$ $s^{-1}$ at the depths of the intrusions and, once the deeper mixing began, minimally $10^{-4}$ $m^2$ $s^{-1}$. Using 0.5 m as a length scale for mixing across the step changes in density, $\tau_{mix}$ is of order 0.5 d (Table 2). Thus, as the plume traverses the lake, vertical mixing will increase its vertical extent with the greatest deepening along the preferential flowpath (Figs. 7, 8, 11). For

**Table 3.** Estimates of retention of DOC-f in the six sub-basins (Fig. 1) and in Toolik Lake as a whole from peak discharge until the end of our sampling under the ice in 2014 and 2015. Retention is defined as the increased number of moles on our final day of sampling to the increased number of moles at the second peak in discharge (*Q*).

| | | 2014 | | | 2015† | | |
|---|---|---|---|---|---|---|---|
| Basin name | Nomenclature | Moles added and retained by the 2nd peak in Q | Moles added and retained by the end of sampling | Retention (%) | Moles added and retained by the 2nd peak in Q | Moles added and retained by the end of sampling | Retention (%) |
| Toolik Inlet Basin | TIB | $6.2 \times 10^4$ | $4.1 \times 10^4$* | 67 | $5.4 \times 10^4$ | $3.3 \times 10^4$ | 61 |
| Toolik Main West | TMW | $1.5 \times 10^5$ | $5.2 \times 10^4$ | 35 | $1.3 \times 10^5$ | $7.8 \times 10^4$ | 62 |
| Toolik Main East | TME | $8.1 \times 10^4$ | $3.6 \times 10^4$ | 45 | $1.3 \times 10^5$ | $6.6 \times 10^4$ | 52 |
| Toolik West | TKW | $1.5 \times 10^5$ | $8.5 \times 10^4$ | 55 | $6.3 \times 10^4$ | $4.5 \times 10^4$ | 72 |
| Toolik East | TKE | $2.1 \times 10^5$ | $1.3 \times 10^5$ | 63 | $1.6 \times 10^5$ | $9.2 \times 10^4$ | 59 |
| Toolik South West | TSW | $6.2 \times 10^4$ | $1.7 \times 10^4$ | 27 | $1.1 \times 10^4$ | $2.9 \times 10^3$ | 27 |
| Whole lake | | $7.2 \times 10^5$ | $3.6 \times 10^5$ | 51 | $5.3 \times 10^5$ | $3.2 \times 10^5$ | 59 |

* So that concentrations in TIB were representative of those introduced through the second peak in discharge, we subtracted the $1.12 \times 10^4$ moles introduced after peak discharge in 2014. Subsequent overflows to other basins were negligible.

† We sampled as discharge was rising and the day after peak discharge in 2015. The increase in cumulative loading from the stream was only 13% over that period, indicating only a small error in our budget.

$l = 3$ m, appropriate to describe erosion at the base of the intrusions, $\tau_{mix}$ is of order a day or less. After peak discharge, when penetrative convection began, $\tau_{mix} < \tau_{adv}$ such that vertical mixing from this mechanism can also redistribute solutes under the ice before the plume exits the lake and contribute to retention (Table 2).

**Retention**

To further evaluate the flowpath in the lake and extent of retention, we use DOC-f as a proxy for solutes, in general, and DOC, in particular. In each basin and for the lake as a whole, we averaged the concentrations of DOC-f at each depth in the lake, multiplied by volume at that depth, and then summed the number of moles (Figs. 7h, 8h; Table 3). We computed average concentration in each basin by dividing the number of moles by the volume of the sub-basin (Figs. 7g, 8g). The magnitude of microbial uptake is low relative to the DOC introduced (Crump et al. 2003). Hence, our budgeting does not include losses by heterotrophic activity. In both years, mean concentrations and the number of moles steadily increased after the first peak in discharge, with $7 \times 10^5$ moles C added and retained by the 2nd peak in discharge in 2014 and $5 \times 10^5$ moles C added and retained in 2015 (Table 3). The different rate of increase in moles of carbon at TME and TKE at peak discharge in 2014 is indicative of the flow of mixed water from the Inlet Basin with its lower concentration of DOC-f to TME and the movement of the still enriched intrusion from TME to TKE. The changes in the western basin, while not as large as to the east, also indicate some dilution of the inflow to TMW and the movement of previously enriched water from TMW to TKW. Mean concentrations and the number of moles decreased after the 2nd peak in discharge. Within a few days, however, mean concentrations and the number of moles in each basin only changed by 5–9%, implying decreased exchange between basins and reduced losses to the outlet. Fifty-one percent of the moles introduced by the second peak in discharge were present by the end of our sampling in 2014 and 59% in 2015 (Table 3). Retention away from the Inlet Basin was higher in 2015 than 2014, reflecting the earlier onset of penetrative convection in that year. The highest retention was to the west, especially in the far northwest where the thinner snowmelt plume enabled an earlier onset of penetrative convection.

We combined the estimates of loading from the stream with the within-lake data to compute retention in 2015 through the end of our under-ice sampling and then through ice-off. The ratio of moles of DOC-f in the lake at the second peak in discharge to the moles of DOC introduced from the stream by that time, $1.58 \times 10^6$ moles C, was 0.34. By multiplying this number by the fractional retention for the subsequent period, 0.59 (Table 3), we estimate 20% of the DOC introduced was retained. The ratio of the $3.2 \times 10^5$ moles C remaining at the end of our sampling to the $2.2 \times 10^6$ moles C introduced by that time gave a similar estimate of retention through the end of our under-ice sampling, 15%. Thus, in 2015, with its rapid melt, a large fraction of the DOC introduced into the lake from the first two peaks in discharge exited. The third discharge event, which occurred close to ice off, also added DOC. The DOC added from the onset of snowmelt through ice off was $3.5 \times 10^6$ moles. At ice off, based on a profile at Toolik Main (T2-2), $4.0 \times 10^5$ moles were in the lake, assuming sufficient spreading in the horizontal for an accurate assessment.

Despite the increase in bacterial productivity as water temperatures warm (Adams et al. 2015), the loss of carbon remains small. Thus, 11% of the DOC introduced into the lake through the full period of snowmelt was retained.

We did not measure loading of DOC in 2014, but we did have profiles of DOC at Toolik Main (T2-2) at peak discharge and immediately after ice off. The close agreement between the profiles of DOC and DOC-f at T2-2 is illustrated in Supporting Information Fig. 2S. Based on the full lake sampling on day 151 under the ice with which we computed moles of DOC-f, and the profile of DOC at ice off which we assume is representative of the lake as a whole given the increased rates of horizontal and vertical mixing when wind could act on the water, we estimate that 54% of the moles which had been introduced at peak discharge were retained. If we assume 35% of the moles introduced by the stream had been retained at peak discharge as in 2015, we estimate $\sim$ 20% retention. These comparisons imply greater retention in years with lower discharge.

The length of time that concentrations in the intrusions remained above ambient depended on weather as it moderated the interval between peaks in discharge. Concentrations were 400 $\mu$M above those in lake water for 2 weeks in 2014 and 4 d in 2015 (Figs. 7, 8). After the second peak in discharge, concentrations remained elevated by $\sim$ 100 $\mu$M for at least the next 10 d in 2014 whereas they were progressively reduced over the next 5 d in 2015.

## Discussion

We present the first comprehensive description of the flowpath of incoming snowmelt waters in an ice-covered lake in the context of weather conditions, variations in discharge, and within-lake stratification. The increased specific conductance and DOC in the initial meltwater flowing into the lake resulted from the preferential elution of solutes in the snow and leaching of organic matter from vegetation and organic rich surface soils (McNamara et al. 1997; Townsend-Small et al. 2011). The concentration of DOC in the incoming stream was twice that in the lake. The density stratification in the lake constrained the incoming snowmelt to flow in a surface boundary layer below the ice. The extent of spreading in the horizontal and development of a preferential flowpath depended on discharge (Fig. 12a,b,c). Once discharge was sufficiently high that incoming water mixed with water in the Inlet Basin, fresher water with a lower concentration of dissolved solutes flowed over the original intrusion with the layered inflows creating step changes in density. The onset and depth of penetrative convection, which contributed to retention, depended on ice thickness and the vertical dimension of the plume (Fig. 12d,e,f). When the melt was rapid, $\sim$ 10% of the incoming DOC was retained through ice off. The fraction increased when the melt was slower. Concentrations of DOC-f in intrusions remained several hundred $\mu$M above those in ambient lake water for $\sim$ 10 d during a rapid melt and over 3 weeks when melt was gradual. In the following, we synthesize results to provide a better understanding of the within lake stratification that moderates the pathway of the inflow and controls on retention. Winter limnology is an understudied subject (Salonen et al. 2009; Bengtsson 2011; Hampton et al. 2016). Results here provide a mechanistic understanding of the hydrodynamics under the ice with implications for biological and chemical processes while lakes are still ice-covered and in the following ice-free period.

The density stratification within the lake and its evolution were critical for determining the flowpath of incoming stream waters. The density structure under the ice depended on temperature, as documented in other northern lakes (Forrest et al. 2008; Salonen et al. 2014; Kirillin et al. 2015) and on specific conductance which is less frequently reported but has been observed in thaw ponds (Deshpande et al. 2015), in Antarctic lakes (Miller and Aiken 1996), and in a few northern lakes (Malm et al. 1998; Kirillin and Terzhevik 2011). The initial increased specific conductance near the surface results from cryoconcentration and that below from respiration primarily within the sediments (Mortimer and Mackereth 1958; Welch and Bergmann 1985). Yearly differences in the stratification of temperature and specific conductance between 3 m and 12 m preconditioned the lake to be more or less receptive to vertical mixing from penetrative convection. These differences likely resulted from conditions during fall which influenced temperatures under the ice and from differences in upwelling vertical velocities (Rizk et al. 2014). Specific conductance will contribute appreciably to density stratification when temperatures are near 4°C in dimictic lakes with high organic matter loading or considerable benthic production in summer followed by respiration or decomposition in winter (e.g., Karlsson et al. 2008).

Several factors influence losses of snowmelt introduced into ice-covered lakes. Water from depths deeper than the outlet will leave the lake. The depth of the outlet changes with discharge, similar to the Inlet, but with a lag. Its depth will also depend on cross-sectional area and bottom roughness. The preferential loss of the shallower, more dilute intrusions, as observed with the second peaks in discharge, contributes to retention (Figs. 7, 8). Additionally, losses would be reduced if vertical mixing deepens the intrusions. Such will occur when $\tau_{mix}$ within the intrusions is less than or equal to $\tau_{adv}$, as we observed (Table 2; Figs. 7, 8). For similar discharge and flow speeds, this time scale analysis indicates plumes would deepen more in longer lakes enabling higher retention. Mixing by penetrative convection would contribute more to retention if it began during high discharge. Thus, factors influencing retention of solutes introduced in the near surface boundary layer at snowmelt include (1) the geometry and changing depth of the outlet stream, (2) the number of peaks in discharge and their

magnitude as they moderate the density of the inflows, layering of intrusions, and their vertical dimension, and (3) the onset, duration and depth of penetrative convection.

Discharge and penetrative convection depend on processes which will change in a warming climate but not necessarily in ways that are predictable now (Lapointe et al. 2016). The onset of penetrative convection depends on ice thickness, which is likely to become less in arctic lakes as precipitation and air temperatures increase in winter. However, winds moderate accumulation of snow on ice and confound predictions (Strum and Liston 2003). Our between year comparisons show the depth of penetrative convection depends on vertical stratification below the surface boundary layer. The processes occurring over the winter which control it are as yet not understood despite careful measurements and modeling (Malm et al. 1998; Rizk et al. 2014; Kirillin et al. 2015). The magnitude and interval between peaks in discharge will affect the duration of intrusions with high concentrations of solutes (Figs. 7, 8). Layers with high concentrations persisted for $\sim$ a month in 2014. In contrast, in 2015, the interval between peaks was short and the high concentrations persisted for a shorter period due to rapid warming and two closely spaced melts. A high pressure system was stationary over northern Alaska at that time. Thus a number of aspects related to weather and the large scale controls on weather affect duration of intrusions with high concentrations of solutes and their overall retention.

Controls on retention in smaller lakes can be predicted from differences in the flowpath in Toolik's sub-basins. For example, cold temperatures forced the initial intrusions to flow under the ice. From the patterns in the Inlet Basin, we can expect that subsequent warming of streams and further increases in density from the interactions of melting snow with soils would cause streams entering small lakes to plunge enabling solute retention. Greater retention is expected when overflows are thin, as in Toolik's far northwestern basin, and penetrative convection is initiated before the introduced solutes exit the lake. Longer advective time scales in small lakes will occur when the outlet is partially blocked by braids or small shrubs, as is common. In addition, seepage over the winter may cause lake levels to decline below the depth of the outlet, which would delay losses. Thus, changes in weather patterns as they moderate the characteristics of the streams and ice thickness will determine between year patterns in retention. Between lake differences will result from attributes of the outlets.

The biological implications of the introduced solutes will depend on whether they are retained as thin layers or mixed extensively. For example, persistent layers in stratified waters in the ocean can be hotspots of biological activity (Alldredge et al. 2002; McManus et al. 2003). Crump et al. (2003)'s results indicate that bacterial productivity at depths influenced by the incoming plume can be as high as measured over the summer despite cold temperatures. While much of the increased productivity in their study can be attributed to incoming terrestrial bacteria, DOC from the stream increases productivity of bacteria within the lake (Crump et al. 2003). Hence, the interleaving of water masses and the vertical mixing within the near surface boundary layer could stimulate within lake microbial communities. The strong near-surface density gradient allows near-surface temperatures to warm faster than those at deeper depths which could further increase microbial activity (Fig. 6) (Adams et al. 2015). Concentrations of $CH_4$ increased in near surface layers from $\sim$ 0.1 $\mu$M to 2 $\mu$M (data not shown) which could energize methanotrophs. The incoming snowmelt water could also provide nutrients to algal communities under the ice; reduced vertical mixing would allow exposure to higher irradiance resulting in overall higher growth (Jewson et al. 2009; Vehmaa and Salonen 2009). Given the increases in DOC and $CH_4$ above ambient in intrusions, the introduced bacteria (Crump et al. 2003), and the constrained vertical mixing, layers below the ice have the potential to be hotspots of activity which may moderate communities and productivity in the ice free season.

The incoming water and its flow under the ice can modify ecosystem structure and function in other ways. With respect to incoming DOC, Crump et al. (2003) illustrate the resulting increased microbial productivity under the ice. The quantity that flows downstream will be photooxidized and contribute to $CO_2$ evasion (Cory et al. 2014). The quantity retained will support increased microbial productivity at ice off with the increase dependent on the remaining labile fractions and lake temperatures (Michaelson et al. 1998; Crump et al. 2003; Adams et al. 2015). It will moderate optical properties with implications for heat budgets and stratification in the ice-free period and availability of light to support benthic production (Ask et al. 2012). Flow under the ice may affect higher trophic levels by moving phytoplankton and associated larval zooplankton toward the lake margins and the outlet (Fig. 3b,e). Their movement could cue juvenile and adult fish to swim to the outlet and ultimately trigger migration. Alternatively, the fish may cue on odors associated with CDOM, the increased temperatures in the near-surface layer, or the higher flow speeds toward the outlet (Heim et al. 2015). Thus, incoming snowmelt waters and associated solutes influence a diverse suite of ecosystem processes.

A considerable quantity of solutes is introduced into lakes during snowmelt. Between year variability in loading may depend on spatial variability in snowmelt and soil warming (Webb et al. 2015). Once snowmelt enters an ice-covered lake, density differences in the vertical moderate the depth of the intruding water, the magnitude of discharge moderates its flowpath, and the initial ice thickness and rate of melt moderate the onset of penetrative convection which retains introduced solutes but may disrupt layered communities. Retention is favored when time scales of vertical mixing are less than

those for advection to the outlet. Continued cool conditions in spring and a slow rate of melt favor retention and the persistence of elevated concentrations of introduced solutes and any associated communities. This mechanistic analysis of the processes moderating the flowpath of the snowmelt plume and retention of solutes enables interpretations at other lakes and generates questions related to system response ranging from hydrodynamics to fish behavior.

## References


Adams, H. E., C. Crump, and G. W. Kling. 2015. Isolating the effects of storm events on arctic aquatic bacteria: Temperature, nutrients, and community composition as controls on bacterial productivity. Front. Microbiol. **6**: 1–13. doi:10.3389/fmicb.2015.00250

Alldredge, A. L., and others. 2002. Occurrence and mechanisms of formation of a dramatic thin layer of marine snow in a shallow Pacific fjord. Mar. Ecol. Prog. Ser. **233**: 1–12. doi:10.3354/meps233001

Ask, J., J. Karlsson, and M. Jansson. 2012. Net ecosystem production in clear-water and brown-water lakes. Global Biogeochem. Cycles **26**: 7. doi:10.1029/2010GB003951

Bengtsson, L. 1986. Dispersion in ice-covered lakes. Nord. Hydrol. **17**: 151–170. doi:10.2166/nh.1986.010

Bengtsson, L. 1996. Mixing in ice-covered lakes. Hydrobiologia **322**: 91–97. doi:10.1007/BF00031811

Bengtsson, L. 2011. Ice-covered lakes: Environment and climate-required research. Hydrol. Process. **25**: 2767–2769. doi:10.1002/hyp.8098

Bergmann, M. A., and H. E. Welch. 1985. Spring meltwater mixing in small arctic lakes. Can. J. Fish. Aquat. Sci. **42**: 1789–1798. doi:10.1139/f85-224

Cai, Y., L. Guo, and T. A. Douglas. 2008. Temporal variations in organic carbon species and fluxes from the Chena River, Alaska. Limnol. Oceanogr. **53**: 1408–1419. doi:10.4319/lo.2008.53.4.1408

Carlson, C. A., A. Hansell, N. B. Nelson, D. A. Siegel, W. M. Smethie, S. Khatiwala, M. M. Meyers, and E. Halewood. 2010. Dissolved organic carbon export and subsequent remineralization in the mesopelagic and bathypelagic realms of the North Atlantic basin. Deep-Sea Res. II **57**: 1433–1445. doi:10.1016/j.dsr2.2010.02.013

Chen, C. T., and F. J. Millero. 1977. The use and misuse of pure water PVT properties for lake waters. Nature **266**: 707–708. doi:10.1038/266707a0

Cory, R. M., C. P. Ward, B. C. Crump, and G. W. Kling. 2014. Sunlight controls water column processing of carbon in arctic fresh waters. Science **345**: 925–928. doi:10.1126/science.1253119

Crump, B. C., W. Kling, M. Bahr, and J. E. Hobbie. 2003. Bacterioplankton community shifts in an Arctic lake correlate with seasonal changes in organic matter source. Appl. Environ. Microbiol. **69**: 2253–2268. doi:10.1128/AEM.69.4.2253

Deshpande, B. N., S. MacIntyre, A. Matveev, and W. F. Vincent. 2015. Oxygen dynamics in permafrost thaw lakes: Anaerobic bioreactors in the Canadian subarctic. Limnol. Oceanogr. **60**: 1656–1670. doi:10.1002/lno.10126

Euskirchen, E. S., S. Bret-Harte, G. J. Scott, C. Edgar, and G. R. Shaver. 2012. Seasonal patterns of carbon dioxide and water fluxes in three representative tundra ecosystems in northern Alaska. Ecosphere **3**: 1–19. doi:10.1890/ES11-00202.1

Farmer, D. M. 1975. Penetrative convection in the absence of mean shear. Q. J. R. Meteorol. Soc. **101**: 869–891. doi:10.1002/qj.49710143011

Forrest, A. L., E. Laval, R. Pieters, D. S. S. Darlene, and D. S. S. Lim. 2008. Convectively driven transport in temperate lakes. Limnol. Oceanogr. **53**: 2321–2332. doi:10.4319/lo.2008.53.5_part_2.2321

Hamblin, P. F., and E. C. Carmack. 1990. On the rate of heat transfer between a lake and an ice sheet. Cold Reg. Sci. Technol. **18**: 173–182. doi:10.1016/0165-232X(90)90006-I

Hampton, S. E., and others. 2016. Ecology under lake ice. Ecol. Lett. **20**: 98–111. doi:10.1111/ele.12699

Heim, K. C., S. Wipfli, M. S. Whitman, C. D. Arp, J. Adams, and J. A. Falke. 2015. Seasonal cues of Arctic grayling movement in a small Arctic stream: The importance of surface water connectivity. Environ. Biol. Fishes **99**: 49–65. doi:10.1007/s10641-015-0453-x

Jakkila, J., M. Leppäranta, T. Kawamura, K. Shirasawa, and K. Salonen. 2009. Radiation transfer and heat budget during the ice season in Lake Pääjärvi, Finland. Aquat. Ecol. **43**: 681–692. doi:10.1007/s10452-009-9275-2

Jassby, A., and T. Powell. 1975. Vertical patterns of eddy diffusion during stratification in Castle Lake, California. Limnol. Oceanogr. **20**: 530–543. doi:10.4319/lo.1975.20.4.0530

Jewson, D. H., G. Granin, A. A. Zhdanov, and R. Y. Gnatovsky. 2009. Effect of snow depth on under-ice irradiance and growth of Aulacoseira baicalensis in Lake Baikal. Aquat. Ecol. **43**: 673–679. doi:10.1007/s10452-009-9267-2

Karlsson, J., J. Ask, and M. Jansson. 2008. Winter respiration of allochthonous and autochthonous organic carbon in a subarctic clear-water lake. Limnol. Oceanogr. **53**: 948–954. doi:10.4319/lo.2008.53.3.0948

Kirillin, G., and A. Terzhevik. 2011. Thermal instability in freshwater lakes under ice: Effect of salt gradients or solar radiation? Cold Reg. Sci. Technol. **65**: 184–190. doi:10.1016/j.coldregions.2010.08.010

Kirillin, G., and others. 2012. Physics of seasonally ice-covered lakes: A review. Aquat. Sci. **74**: 659–682. doi:10.1007/s00027-012-0279-y

Kirillin, G. B., A. Forrest, K. Graves, A. Fischer, C. Engelhardt, and B. E. Laval. 2015. Axisymmetric circulation driven by

marginal heating in ice-covered lakes. Geophys. Res. Lett. **42**: 2893–2900. doi:10.1002/2014GL062180

Lapointe, F., P. Francus, S. F. Lamoureux, M. Vuille, J.-P. Jenny, and R. S. Bradley. 2016. Influence of North Pacific decadal variability on the western Canadian Arctic over the past 700 years. Clim. Past 1–14. doi:10.5194/cp-2016-118

Luecke, C., and others. 2014. The response of Lakes near the Arctic LTER to environmental change, p. 238–286. *In* J. Hobbie and G. Kling [eds.], A changing arctic: Ecological consequences for tundra, streams and lakes. Oxford Univ. Press.

MacIntyre, S., K. M. Flynn, R. Jellison, and J. Romero. 1999. Boundary mixing and nutrient fluxes in Mono Lake, California. Limnol. Oceanogr. **44**: 512–529. doi:10.4319/lo.1999.44.3.0512

Macintyre, S., J. O. Sickman, S. A. Goldthwait, and G. W. Kling. 2006. Physical pathways of nutrient supply in a small, ultraoligotrophic arctic lake during summer stratification. Limnol. Oceanogr. **51**: 1107–1124. doi:10.4319/lo.2006.51.2.1107

MacIntyre, S., J. P. Fram, P. J. Kushner, N. D. Bettez, W. J. O. Brien, J. E. Hobbie, and G. W. Kling. 2009. Climate-related variations in mixing dynamics in an Alaskan arctic lake. Limnol. Oceanogr. **54**: 2401–2417. doi:10.4319/lo.2009.54.6_part_2.2401

Malm, J., L. Bengtsson, A. Terzhevik, P. Boyarinov, A. Glinsky, N. Palshin, and M. Petrov. 1998. Field study on currents in a shallow, ice-covered lake. Limnol. Oceanogr. **43**: 1669–1679. doi:10.4319/lo.1998.43.7.1669

McManus, M. A., and others. 2003. Characteristics, distribution and persistence of thin layers over a 48 hour period. Mar. Ecol. Prog. Ser. **261**: 1–19. doi:10.3354/meps261001

McNamara, J. P., L. Kane, and L. D. Hinzman. 1997. Hydrograph separations in an arctic watershed using mixing model and graphical techniques. Water Resour. Res. **33**: 1707. doi:10.1029/97WR01033

McNamara, J. P., L. Kane, J. E. Hobbie, and G. W. Kling. 2008. Hydrologic and biogeochemical controls on the spatial and temporal patterns of nitrogen and phosphorus in the Kuparuk River, arctic Alaska. Hydrol. Process. **22**: 3294–3309. doi:10.1002/hyp.6920

Michaelson, G. J., L. Ping, G. W. Kling, and J. E. Hobbie. 1998. The character and bioactivity of dissolved organic matter at thaw and in the spring runoff waters of the arctic tundra North Slope, Alaska. J. Geophys. Res. **103**: 28939. doi:10.1029/98JD02650

Miller, L. G., and G. R. Aiken. 1996. Effects of glacial meltwater inflows and moat freezing on mixing in an ice-covered Antarctic lake as interpreted from stable isotope and tritium distributions. Limnol. Oceanogr. **41**: 966–976. doi:10.4319/lo.1996.41.5.0966

Mironov, D. V., and A. Y. Terzhevik. 2000. Spring convection in ice-covered freshwater lakes. Atmos. Ocean. Phys. **36**: 681–688. doi:10013/epic.14718

Moore, R. D. D. 2005. Slug injection using salt in solution. Streamline Watershed Manag. Bull. **8**: 1–6.

Mortimer, C. H., and F. J. H. Mackereth. 1958. Convection and its consequences in ice-covered lakes. Verhandlungen Des Int. Verein Limnol. **13**: 923–932.

O'Brien, W. J., and others. 1997. The limnology of Toolik Lake, p. 61–106. *In* A. M. Milner and M. W. Oswood [eds.], Freshwaters of Alaska. Springer.

Pieters, R., and G. A. Lawrence. 2009. Effect of salt exclusion from lake ice on seasonal circulation. Limnol. Oceanogr. **54**: 401–412. doi:10.4319/lo.2009.54.2.0401

Rizk, W., G. Kirillin, and M. Lepparanta. 2014. Basin-scale circulation and heat fluxes in ice-covered lakes. Limnol. Oceanogr. **59**: 445–464. doi:10.4319/lo.2014.59.02.0445

Rueda, F. J., and S. MacIntyre. 2009. Flow paths and spatial heterogeneity of stream inflows in a small multibasin lake. Limnol. Oceanogr. **54**: 2041–2057. doi:10.4319/lo.2009.54.6.2041

Rueda, F. J., and S. MacIntyre. 2010. Modelling the fate and transport of negatively buoyant storm-river water in small multi-basin lakes. Environ. Model. Softw. **25**: 146–157. doi:10.1016/j.envsoft.2009.07.002

Salonen, K., M. Leppäranta, M. Viljanen, and R. D. Gulati. 2009. Perspectives in winter limnology: Closing the annual cycle of freezing lakes. Aquat. Ecol. **43**: 609–616. doi:10.1007/s10452-009-9278-z

Salonen, K., M. Pulkkanen, P. Salmi, and R. W. Griffiths. 2014. Interannual variability of circulation under spring ice in a boreal lake. Limnol. Oceanogr. **59**: 2121–2132. doi:10.4319/lo.2014.59.6.2121

Sengers, J. V., and J. T. R. Watson. 1986. Improved international formulations for the viscosity and thermal conductivity of water substance. J. Phys. Chem. Ref. Data **15**: 1291–1314. doi:10.1063/1.555763

Sickman, J. O., A. Leydecker, C. C. Y. Chang, C. Kendall, J. M. Melack, D. M. Lucero, and J. Schimel. 2003. Mechanisms underlying export of N from high-elevation catchments during seasonal transitions. Biogeochemistry **64**: 1–24. doi:10.1023/A:1024928317057

Stigebrandt, A. 1978. Dynamics of an ice covered lake with through-flow. Hydrol. Res. **9**: 219–244.

Strum, M., and G. E. Liston. 2003. The snow cover on lakes of the Arctic Coastal Plain of Alaska, U.S.A. J. Glaciol. **49**: 370–380. doi:10.3189/172756503781830539

Sturman, J. J., N. Ivey, and J. R. Taylor. 1996. Convection in a long box driven by heating and cooling on the horizontal boundaries. J. Fluid Mech. **310**: 61. doi:10.1017/S0022112096001735

Townsend-Small, A., J. W. McClelland, R. M. Holmes, and B. J. Peterson. 2011. Seasonal and hydrologic drivers of dissolved organic matter and nutrients in the upper Kuparuk

River, Alaskan Arctic. Biogeochemistry **103**: 109–124. doi: 10.1007/s10533-010-9451-4

Vehmaa, A., and K. Salonen. 2009. Development of phytoplankton in Lake Pääjärvi (Finland) during under-ice convective mixing period. Aquat. Ecol. **43**: 693–705. doi: 10.1007/s10452-009-9273-4

Virtanen, M., J. Forsius, and J. Sarkkula. 1979. The ice covered circulation in Lake Pyhäjärvi near Tampere. Proc. Nord. Work. Dyn. Lakes **2**: 317–322.

Webb, R. W., R. Fassnacht, and M. N. Gooseff. 2015. Wetting and drying variability of the shallow subsurface beneath a snowpack in California's Southern Sierra Nevada. Vadose Zone J. **14**: 1–10. doi:10.2136/vzj2014.12.0182

Welch, H. E., and M. A. Bergmann. 1985. Water circulation in small Arctic lakes in winter. Can. J. Fish. Aquat. Sci. **42**: 506–520. doi:10.1139/f85-068

Wetzel, R. G., and G. E. Likens. 2000. Limnological analyses, 3rd ed. Springer.

Whalen, S. C., and J. C. Cornwell. 1985. Nitrogen, phosphorus, and organic carbon cycling in an Arctic lake. Can. J. Fish. Aquat. Sci. **42**: 797–808. doi:10.1139/f85-102

## Acknowledgments

We thank Jade Lawrence, Erik Young, Analisa Skeen, Katie Ringler, Jeb Timm, Joe Franich, Caitlin Rushlow, Ricardo Roman Botero, Andres Gomez-Giraldo, Adam Crowe, John Lenters, and John Melack for their help with field measurements and laboratory analysis, and Chris Gotschalk and Adam Crowe for assistance with processing and analysis of physical data. We thank Fabian Wolk and Rockland Scientific for the loan of the JFE Advantech CTD plus Rinko for the 2014 spring field season and Michael Head of PME for adapting the SCAMP for under-ice profiling. We thank Jason Stuckey and Randy Fulweber for the bathymetrical data, and the ARC LTER for time series pressure, temperature, and conductivity data in Toolik Inlet and major ions in inflowing streams. We thank Ellie Wallner of the Carlson laboratory at UCSB for processing DOC samples and Delores Lucero of the Sickman laboratory at UC Riverside for processing the major ion samples. John Melack and two anonymous reviewers critically read the manuscript. Meteorological datasets provided by the Toolik Field Station Environmental Data Center are based upon work supported by the U. S. National Science Foundation (NSF) under grants #455541 and #1048361. The ARC LTER was funded by NSF DEB-1026843. Snow depth was provided by the Institute of Arctic Biology (IAB), UAF, based upon work supported by the NSF under grant #1107892. Logistic support provided by UAF IAB Toolik Field Station was funded by NSF PLR 1048361. User days at Toolik Field Station were provided by CH2M Polar Services through the NSF's Arctic Research Support and Logistics Program grants #1204267 and #0919603. SS received additional postdoctoral support from NSF EAR 1249769. This project was supported by NSF Arctic Natural Sciences (ARC) Grant #120426 to SM.

## Conflict of Interest

None declared.

*Submitted 20 August 2016*
*Revised 08 December 2016*
*Accepted 31 January 2017*

*Associate editor: Craig Stevens*